Water Resources Research

RESEARCH ARTICLE
10.1029/2022WR032842

ICESat-2 Based River Surface Slope and Its Impact on Water Level Time Series From Satellite Altimetry

Daniel Scherer[1], **Christian Schwatke**[1], **Denise Dettmering**[1], **and Florian Seitz**[1]

[1]Department of Aerospace and Geodesy, TUM School of Engineering and Design, Deutsches Geodätisches Forschungsinstitut der Technische Universität München (DGFI-TUM), Munich, Germany

Key Points:

- Simultaneous obs. from Ice, Cloud, and Land Elevation Satellite 2's (ICESat-2's) unique multibeam lidar altimeter are used to estimate instantaneous reach-scale water surface slope (WSS)
- For 89% of 815 studied reaches, we find ICESat-2 can be used to estimate WSS with a median absolute error of 23 mm/km relative to gauge data
- We correct water level time series from radar satellite altimetry for the derived WSS and obtain improvements of up to 30 cm (66%) root mean square error

Correspondence to:
D. Scherer,
daniel.scherer@tum.de

Citation:
Scherer, D., Schwatke, C., Dettmering, D., & Seitz, F. (2022). ICESat-2 based river surface slope and its impact on water level time series from satellite altimetry. *Water Resources Research*, *58*, e2022WR032842. https://doi.org/10.1029/2022WR032842

Received 8 JUN 2022
Accepted 25 OCT 2022

Author Contributions:
Conceptualization: Daniel Scherer
Data curation: Christian Schwatke
Funding acquisition: Denise Dettmering, Florian Seitz
Methodology: Daniel Scherer
Project Administration: Denise Dettmering, Florian Seitz
Software: Daniel Scherer
Supervision: Denise Dettmering, Florian Seitz
Validation: Daniel Scherer
Visualization: Daniel Scherer
Writing – original draft: Daniel Scherer

Abstract The water surface slope (WSS) of rivers is essential for estimating flow velocity and discharge. It is also helpful as a correction applied to range measurements of satellite altimetry missions to derive water level time series at a virtual station. Using radar altimetry, WSS can only be roughly estimated and is limited to wide rivers because of its coarse spatiotemporal resolution. In contrast, the lidar sensor onboard Ice, Cloud, and Land Elevation Satellite 2 (ICESat-2) can also observe small rivers. Using ICESat-2's unique measurement geometry with six parallel laser beams, we derive instantaneous WSS along and across the satellite's ground track, time-variable WSS (with an average of 5 days of records in the studied epoch between October 2018 and October 2021), and average WSS on reach-scale. Although the method can be applied globally, this study is limited to 815 reaches in Europe and North America where sufficient validation data is available. We compare the ICESat-2 WSS with time-variable WSS derived from multiple gauges and constant data from the "SWOT River Database." For 89% of the studied reaches, ICESat-2 can be used to estimate the average WSS with a median absolute error of 23 mm/km. We also show the possible performance gain at multiple virtual stations (VS) in the "Database for Hydrological Time Series of Inland Waters" (https://dahiti.dgfi.tum.de), applying the WSS as a correction for altimetry satellites' ground track variability. We correct 137 VS for the derived ICESat-2 WSS and yield improvements in the root mean square error by up to 30 cm or 66%.

1. Introduction

The water surface slope (WSS), hydraulic gradient, or flow gradient of a river is the slope of the hydraulic grade line, that is, the change of the pressure head per distance unit (Gliński et al., 2011; Herrmann & Bucksch, 2014; Julien, 2018b). It is typically defined positive for an decreasing water surface elevation (WSE) in downstream direction (Julien, 2018b). WSS is not stationary but changes over time and space. Especially in natural rivers that are non-uniform and unsteady, the WSS is variable over time because of morphological changes of the river bed and flood waves (Julien, 2018a). Locally, WSS may differ from larger-scale averages and change with every reach because of local characteristics like cascades, pools, or tributary estuaries (Rhoads, 2020; Schumm, 2005). While the WSS of an alluvial river is gradual, bedrock causes natural discontinuities in semi-alluvial rivers (Julien, 2018b). In hydrology, WSS is a critical parameter required to calculate flow velocity and discharge (Manning, 1891; Rhoads, 2020). The flow velocity derived from WSS is also essential for densifying spatial or temporal low-resolution water level measurements from non-repeating satellite altimetry missions such as Cryosat-2 (Tourian et al., 2016). Generally, the WSS can be used to correct any satellite altimetry mission to compensate for the satellites' ground track variability when calculating long-term water level time series at fixed locations, so-called virtual stations (VS).

WSE measurements of the "Shuttle Radar Topography Mission" (SRTM) are regularly used to derive WSS (Cohen et al., 2018; Kebede et al., 2020; LeFavour & Alsdorf, 2005; Sichangi et al., 2018). However, because of its relatively large height error, WSS estimates from SRTM data are only appropriate on a large scale (LeFavour & Alsdorf, 2005). For river discharge estimation and satellite altimetry correction, though, smaller-scale WSS are favorable. Additionally, SRTM captured only a short epoch of 11 days in February 2000, and the WSS observed during this time may not represent the respective average WSS.

There are only a few methods capable of detecting small-scale local changes of WSS with high resolution. Airborne lidar (Mandlburger et al., 2020) and radar (Jiang et al., 2020) sensors or measurements from field campaigns (Carr et al., 2019; Pitcher et al., 2020) are suitable because of the continuous local mapping of the WSE. However, such airborne or field campaigns require significant personnel and cost-intensive effort, so they

Writing – review & editing: Christian Schwatke, Denise Dettmering, Florian Seitz

can only be applied occasionally to selected reaches but are not suitable to continuously observe the WSS of an entire river system. Therefore, the WSS observations may not agree with the actual average WSS, similar to methods using SRTM data.

Better suited for operational usage, WSE measurements between two stations, such as gauges, with a known distance along the river and without flow disturbances in between can be used to estimate WSS. The local scales depend on the distribution of stations along the river. Although such WSS estimates represent only a mean between the stations and small-scale deviations may not be captured, temporal changes of the long-term mean WSS can be monitored by the temporal continuous WSE measurements.

In-situ gauging stations are the most accurate WSE sources as the pressure head is continuously measured by a probe in a housing sheltered from disturbances, for example, weather (Sauer & Turnipseed, 2010). However, maintaining a network of gauging stations is challenging (Calmant & Seyler, 2006), limiting the number of monitored sites and increasing the probability of undetected flow disturbances or significant changes in WSS between two gauges. Therefore, WSS estimates between two in-situ stations may not always be meaningful, especially, when both stations do not reference the same vertical datum. Often, gauge data can not be used to derive WSS because the vertical datum is not specified. Additionally, from a global view, the spatial distribution of gauges is uneven, concentrated in developed countries and absent in remote areas, which is apparent from the availability of the derived discharge data (Hannah et al., 2011).

In contrast, satellite altimetry provides homogeneously distributed data globally. However, the number of potential VS depends on the satellite orbit and how the track crosses a river of interest. It may miss meridional flowing rivers parallel to its ground track or cross meandering rivers multiple times within a short distance. Overall, the temporal resolution of WSE measurements by satellite altimetry is significantly lower than that of gauges. Classical pulse-limited radar or low-resolution mode (LRM) altimeters measure only in nadir direction and may have a significant error for narrow rivers due to the large radar footprint (Calmant et al., 2016). Still, for rivers wider than 200 m the WSE can be derived from LRM altimetry with an root mean square error (RMSE) of a few decimeters (Schwatke et al., 2015; Sulistioadi et al., 2015). WSE measurements using synthetic aperture radar (SAR) can be used for rivers that are up to 40 m narrow with similar accuracy (Halicki & Niedzielski, 2022), and the more modern techniques like interferometric SAR (SARIn) and laser altimeters are still more accurate and applicable for even more narrow rivers. Furthermore, modern sensors such as the planned "Surface Water and Ocean Topography" (SWOT) mission measure not only in nadir direction but within a swath so that WSS can be instantaneously derived within one pass (Langhorst et al., 2019).

Despite the challenges and uncertainties, satellite altimetry is widely used to estimate WSS, predominantly to derive river discharge (Gleason & Durand, 2020; Sichangi et al., 2016). In a study for two arctic rivers, SARIn and SAR data from the CryoSat-2, SARAL, and Sentinel-3A missions were used to model the longitudinal river profile using a time-variable cubic spline function (Zakharova et al., 2020). In this way, it was possible to estimate WSS at any location and time for a 175 km segment of the Ob River. However, no satisfactory satellite altimetry data could be retrieved for the Pur River. The average relative model error was 22%, with error estimates ranging from 1.4 to 10 mm/km for WSS between 1 and 13 mm/km. However, the authors state these errors might be underestimated. A linear model was used to derive constant WSS of the Mississippi River with a least-squares approach based on Jason-2/-3, ENVISAT ("Environmental Satellite"), and Sentinel-3A/B data (Scherer et al., 2020). The average absolute median deviation of the WSS between the VS compared to the WSS measurements between seven gauges was 12 mm/km with a median relative error of 19.4%. WSS could also be derived from a topographic model of the Mekong River which used B-Splines on a directed tree graph fitted to multi-mission satellite altimetry WSE observations (Boergens et al., 2021). However, the model was limited by the uneven distribution of observations and quality suffered in regions with sparse data.

Without applying a model, WSE differences between consecutive intersections of the same satellite altimetry passes with two reaches of the Yukon River were used to estimate WSS (Bjerklie et al., 2018). The resulting WSS ranged between 30 and 140 mm/km and were within the range of 10–320 mm/km observed by field measurements. In a similar way, WSS was determined for the Xingu River using WSE measurements of 10 consecutive crossings of the ENVISAT mission (Garambois et al., 2017). Although these studies may yield good results, methods using consecutive crossings of one satellite altimetry pass are limited to a small number of sites by the orbit geometry of the respective mission. In contrast, ICESat data of different passes observed within 2 days difference were used to estimate WSS for the Congo River (O'Loughlin et al., 2013). Because of the long repeat

cycle of ICESat, it is more likely to get useable data for any global river with this method. However, there may be errors introduced due to the time lag between the asynchronous WSE observations.

In this paper, we use WSE measurements acquired by the follow-on mission of ICESat, the "Ice, Cloud, and Land Elevation Satellite 2" (ICESat-2). Similar to ICESat, it is placed on a long-repeat orbit and therefore, covers many reaches but revisits them only every 91 days. Compared to ICESat, the coverage of ICESat-2 is increased by its new sensor, the "Advanced Topographic Laser Altimeter System" (ATLAS), which measures the Earth's topography along the ground track of three parallel pairs of laser beams spaced 3.3 km apart (Markus et al., 2017; Neumann et al., 2019). This increases the probability of simultaneous WSE measurements at different locations within a river reach.

The novel approach presented in this study uses ICESat-2's unique measurement geometry to derive instantaneous reach-scale river WSS. Two methods, (a) the across-track and (b) the along-track, are combined in this approach. In the across-track method, we calculate the WSS between the simultaneous WSE measurements of ICESat-2's parallel beams intersecting a reach. Additionally, we fit the WSS to all WSE observations of each individual beam intersecting the river reach and project it to the river centerline in the along-track method. Both methods are combined into a time-variable WSS to maximize the temporal and spatial coverage. Furthermore, an average reach-scale WSS is computed. In this way, we aim to derive global average reach-scale WSS and its variability in future studies.

Amongst other data required for this study, the used ICESat-2 data set is described in Section 2. The approach to derive WSS is described in Section 3. The resulting WSS are compared with time-variable WSS between in-situ gauges in Section 4 where we also show the impact of applying the reach-scale WSS as a correction to VS hydrographs.

2. Study Areas and Data

For this study, we select rivers in Europe and North America where a sufficient number of in-situ data are available for validation. The maps of these regions (Figure 1) contain all reaches defined by the "SWOT River Database" (SWORD, see Section 2.2). Only the bold reaches are studied in this paper because the selection of the studied reaches is limited by the availability of in-situ gauges suitable for validation and their connectivity so that there are no dams, weirs, major riffles, or confluences in between the gauges. All the in-situ sources are given in Section 2.3. No WSS can be derived for the purple reaches because no or insufficient data is available from ICESat-2. The ICESat-2 data is described in Section 2.1. Table A1 in the appendix lists the characteristics of the studied river sections according to SWORD and the in-situ sources used which we describe in Section 2.3. Although strongly limited by the spatial distribution of suitable gauges, we include as diverse reaches as possible, especially regarding the nominal slope and width. Figure 1 also shows the orbit ground tracks of the Jason-2/3 and Sentinel-3A/B missions and the VS used in this study. We describe the radar satellite altimetry data in Section 2.4.

2.1. ATLAS/ICESat-2 ATL13 L3A Inland Water Surface Height Product

The primary data used in this study are WSE measurements acquired by ICESat-2 provided within the "ATLAS/ICESat-2 L3A Along Track Inland Surface Water Data" (ATL13) (Jasinski et al., 2021b) product by the "National Snow & ICE Data Center" (NSIDC). The satellite is placed on a 91-day repeat orbit with an inclination of 92° (Markus et al., 2017). The ATLAS sensor onboard ICESat-2 is a photon-counting lidar, measuring the time an emitted photon travels to Earth and back to the sensor. ATLAS emits photons along three pairs of beams, which each consist of a high energy (175 ± 17 μJ) "strong" beam and a low energy (45 ± 5 μJ) "weak" beam. Each beam illuminates a footprint of approximately 17 m in diameter at a pulse rate of 10kHz (i.e., one pulse every 0.7 m) (Neumann et al., 2019). However, because of the low reflectance of water, a maximum of 2.9 photons per meter can be observed by the sensor over inland waters, depending on the water and atmospheric conditions (Jasinski et al., 2021a).

Two global studies (Cooley et al., 2021; Ryan et al., 2020) validate the "ATLAS/ICESat-2 L3A Land and Vegetation Height (ATL08)" data, which reportedly contain very similar water level observations to the ATL13 data (Ryan et al., 2020). For lakes and reservoirs, there is no significant difference in the accuracy between the strong and weak beams (Cooley et al., 2021). In contrast to radar altimetry, the lidar sensor can not penetrate clouds, so

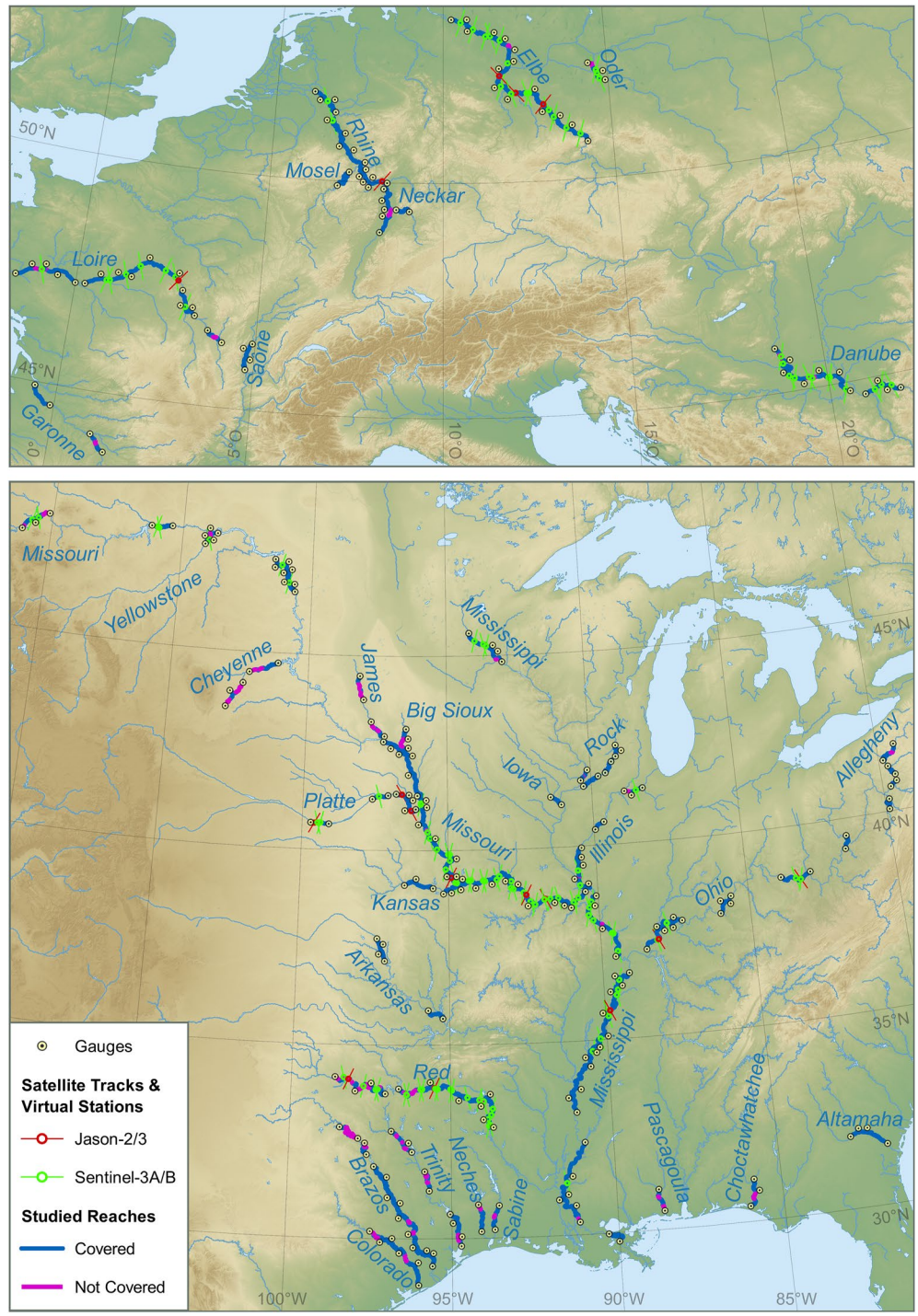

Figure 1. Regions with studied reaches, in-situ gauges we use for validation, and virtual stations to which we apply the water surface slope correction. Top: Europe. Bottom: North America.

there are missing observations in overcast conditions. The median standard deviation of ICESat-2 observations over inland waters is reported to be 0.017 m, with a mean error of 0.14 m (Cooley et al., 2021; Ryan et al., 2020). A regional study validating ATL13 data at the Mekong River reports similar results with an RMSE of 0.24 m and a median standard deviation of 0.04 m (Lao et al., 2022).

The ATL13 product does not contain photon-level observations but representative values over short segments of 75–100 consecutive received photons above inland water bodies. These short segments have an along-track length of 30 to several hundred meters, depending on the number of received signal photons per pulse. In this paper, we use the "ht_water_surf" parameter, the mean water surface height, with reference to the WGS84 ellipsoid per beam and short segment (Jasinski et al., 2021a). We apply the EIGEN-6C4 geoid (Foerste et al., 2014) to have a common reference of the ICESat-2 WSE data with other satellite altimetry data used in this study. Additionally, we use the spacecraft orientation parameter to identify the strong and weak beams and compare the respective results.

2.2. SWOT River Database (SWORD)

To determine the angle and chainage at which the beam ground tracks of ICESat-2 intersect a river, we use the high-resolution (30 m) river centerlines from SWORD (Version v1) (Altenau et al., 2021a). SWORD is based on the "Global River Widths from Landsat" (GRWL) data set (Allen & Pavelsky, 2018), which contains river centerlines processed from Landsat imagery at mean annual flow. For SWORD, the GRWL centerlines were segmented at natural and artificial river obstructions, basin boundaries, tributary junctions, or otherwise approximately every 10 km. SWORD also includes data on river obstructions and topology, which we use to determine whether two stations are connected without flow disturbances in between. Additionally, SWORD contains constant WSS data per reach, which we use as a benchmark to compare our results besides in-situ gauging data. The SWORD WSS are estimated by fitting a linear regression to elevation data from the MERIT Hydro data set (Altenau et al., 2021a; Yamazaki et al., 2019). MERIT Hydro is derived from MERIT DEM which comprises remote sensing data from the SRTM and "Advanced Land Observing Satellite" (ALOS) missions, with removed noise, height errors, and tree canopy biases (Yamazaki et al., 2017). Furthermore, SWORD contains the width of each reach at mean annual flow, which we use to filter the ICESat-2 observations.

2.3. In-Situ Water Level Time Series From Gauges

We validate the WSS using in-situ WSE data observed at multiple pairs of gauges. The in-situ data of single gauges are also used to determine error measures for satellite-derived hydrographs at VS before and after applying the WSS as a correction. We retrieve the in-situ data for Germany from the "Wasserstraßen- und Schifffahrtsverwaltung des Bundes" (WSV) provided by the "Bundesanstalt f"ur Gewässerkunde" (BfG), for the United States from the "U.S. Army Corps of Engineering" (USACE) and the "U.S. Geological Survey" (USGS), for France from "Hydroportail", and for Serbia from the "Republic Hydrometeorological Service of Serbia" (HIDMET). The number of gauges per river and their vertical datum is listed for each source in Table A1 in the appendix. We only use in-situ data from gauges with a given vertical datum to get an accurate WSE difference between a pair of gauges. In case the given vertical datum varies per gauge within a source, it is converted to the common datum given in Table A1. If a conversion is not possible, the gauge is discarded.

2.4. DAHITI Water Level Time Series From Radar Altimetry

We use water level time series derived from radar satellite altimetry data from the "Database for Hydrological Time Series of Inland Waters" (DAHITI, www.dahiti.dgfi.tum.de) (Schwatke et al., 2015) in this study. The data is provided at VS, which are located at the intersections of a satellite's orbit ground track with a river. We select the Jason-2/3 and Sentinel-3A/B missions for this study. These satellites orbit Earth in a repeating pattern, revisiting the same location every 10 and 27 days, respectively. However, the orbit repeatability at the equator crossing of altimetry satellites is designed to be within ± 1 km (Tapley et al., 1994) so that the exact location where they cross a river is not stationary. For the selected missions, the empirical repeatability magnitude is in a range of 1.5–1.7 km. With a global median river WSS of 469 mm/km (Frasson et al., 2019), these slight deviations at the assumed to be stationary VS can cause a WSE error of up to 1 m on average.

The Jason-2/3 satellites are equipped with a LRM altimeter, which scans a circular area with a diameter of several kilometers (Calmant et al., 2016). Special retracking software must be used for smaller rivers to treat the so-called "hooking" or "off-nadir" effect and signal noise caused by ambient topographic features (Boergens et al., 2016; Frappart et al., 2006; Schwatke et al., 2015). The sensor onboard Sentinel-3A/B is a SAR altimeter, which has an improved along-track resolution of about 300 m (Calmant et al., 2016). Atmospheric, geophysical, and

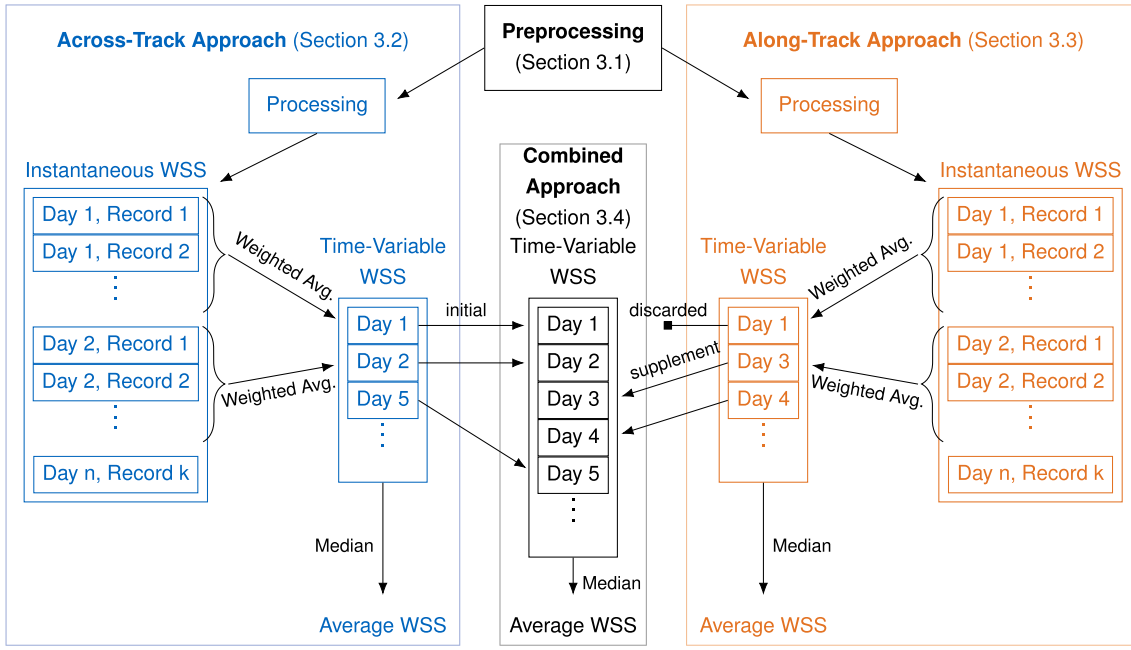

Figure 2. Processing flow and data structure. After preprocessing (Section 3.1) the instantaneous water surface slope (WSS) is estimated using the across-track (blue, Section 3.2) and along-track (orange, Section 3.3) approach. The results are reduced to a time-variable WSS with daily resolution using a weighted average. Both approaches are combined (black, Section 3.4) using the across-track time-variable data supplemented by the along-track data while duplicate along-track data is discarded. An average value is derived for each approach by calculating the median of each time-variable WSS.

instrument corrections must be applied to estimate accurate WSE from satellite altimetry measurements (Calmant et al., 2016). All mutual and satellite-specific corrections are already applied to the time series data retrieved from DAHITI. Additionally, the DAHITI data are corrected by inter-mission biases from a multi-mission cross-over analysis to allow the combination of WSE data from different missions (Bosch et al., 2014; Schwatke et al., 2015).

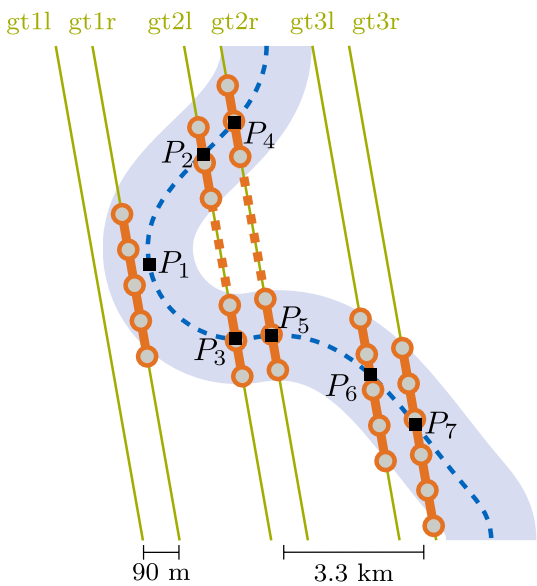

Figure 3. Schematic of Ice, Cloud, and Land Elevation Satellite 2 ATL13 observations (circles) of one cycle within a reach area of interest (light-blue polygon), segmented as features (orange) per beam (green) with reference points (squares) at the centerline (dashed blue) intersections or the nearest centerline point. Features with multiple intersections (dashed orange) are split.

3. Methodology

In this paper, we use two methods to estimate instantaneous, time-variable, and average reach-scale WSS from ICESat-2 observations: (a) Across-track WSE differences of two beams (Section 3.2) and (b) along-track WSE linear trends of single beams (Section 3.3). Both methods have advantages and disadvantages depending on the intersection angle of the orbit ground track with the reach centerline. Therefore, we also estimate time-variable and average WSS using a combined approach (Section 3.4). Figure 2 shows the processing flow and data structure after preprocessing.

3.1. Preprocessing

The processing is performed for each given SWORD reach and starts by selecting all ATL13 observations within the reach area of interest (AOI). To construct the reach AOI, we buffer the SWORD reach center line by the reach's width plus four times its width standard deviation. The AOI of a schematic river reach is shown in Figure 3 as a light-blue polygon. Each beam and cycle of the ATL13 data intersecting with the AOI is handled as an individual feature. Each feature is intersected with the SWORD reach centerline to determine the intersection location as feature reference point P_i and its chainage. In case there are multiple intersections, the feature is split in between.

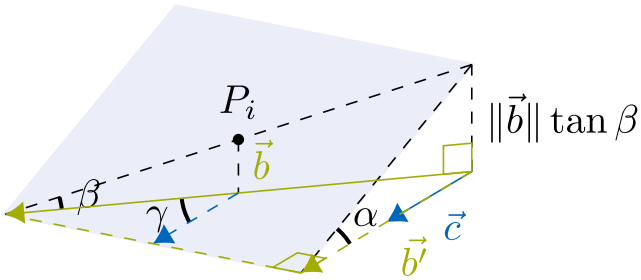

Figure 4. Schematic of an Ice, Cloud, and Land Elevation Satellite 2 beam ground track $\vec{b}$ crossing a river (blue polygon) with centerline tangent vector $\vec{c}$ at an angle γ, along-track water surface slope (WSS) ($\tan\beta$), and along-river WSS ($\tan\alpha$).

If a feature is not intersecting the river centerline, the nearest point of the centerline to the feature is taken as the reference point P_i. Figure 3 shows a schematic of the feature definition with a significantly reduced number of observations for simplicity.

We use the WSE of the already preprocessed ATL13 inland water body height data. Outliers within each feature are detected and removed similar to the DAHITI approach (Schwatke et al., 2015). For this purpose, an absolute deviation around the median (ADM) is calculated using a rolling window along the beam ground track. The windows size is seven observations for features with more than 20 data points across the river. Otherwise, the ADM of all observations is used. All observations with an ADM of more than 5 cm are assumed to be outliers and rejected. Additionally, we use the type ("inland_water_body_type") and cloud ("cloud_flag_asr_atl09") flags from the ATL13 data. Observations, which are not flagged as reservoir, river, or estuary are rejected as well as observation marked cloudy with at least low confidence (flags 0–3). If there are along-track gaps of more than 500 m in the remaining observations, we split the data into clusters at these gaps and use only the cluster with the largest number of observations. Further outliers are detected using a linear support vector regression (SVR). Contrary to the standard DAHITI approach (Schwatke et al., 2015) for radar altimetry, we do not use a zero-slope constraint for the SVR. WSE observations that deviate more than 5 cm from the SVR fit are rejected as outliers.

3.2. Across-Track WSS Estimation

For each feature reference position P_i, we calculate a reference WSE using the average of the valid WSE observations weighted by their inverse distance to P_i. Next, the chainage difference between all possible pairs of reference positions P_i of the same cycle, so also between features of the same beam (e.g., P_4 and P_5 in Figure 3), are calculated. Pairs of reference positions with a chainage distance below 1,000 m are disregarded, assuming the baseline is too short for estimating a meaningful WSS. Between the remaining pairs of reference positions, the WSS is calculated by dividing their WSE difference by their chainage difference. Negative WSS estimates are rejected assuming outliers. In order to reduce the multiple instantaneous results to a reach scale time-variable across-track WSS with daily temporal resolution (i.e., a WSS time series, cf. Figure 2), the daily weighted average is used. The weights are defined as the inverse of the sum of the standard deviations of the WSE observations in both features used to calculate the instantaneous WSS records. In this step samples from different locations within the reach are combined and treated as if the WSS is not changing over the reach. While this does not reflect the real behavior of a river, we assume the SWORD reaches to be homogeneous so that the local WSS variability is of minor significance. Additionally, we derive an average reach-scale across-track WSS by calculating the median of the time-variable WSS values.

3.3. Along-Track WSS Estimation

The spatial resolution of the ICESat-2 ATLAS instrument is high enough (approx. 0.7 m (Jasinski et al., 2021a)) to detect along-track water level differences with small error (approx. 0.061 m (Jasinski et al., 2021a)) in cloud-free conditions within a single river crossing of a beam, respectively one feature (the ATL13 observations assigned to a reference position P_i). Figure 4 shows a schematic of such a feature. Because of the high spatial resolution, precision, and accuracy, we can estimate the along-track WSS ($\tan\beta$) by fitting a linear regression to the ATL13 short segment WSE observations and their along-track position. We use a fitting instead of the difference of the maximum and minimum WSE to cope with undetected outliers. However, for hydraulic applications, the along-river WSS ($\tan\alpha$) is required instead of $\tan\beta$. In order to estimate $\tan\alpha$ at a reference position P_i, the vector of the features beam ground track segment $\vec{b}$ is projected onto the river centerline tangent vector $\vec{c}$:

$$\vec{b'} = \frac{\vec{b} \cdot \vec{c}}{\|\vec{c}\|^2} \vec{c} \tag{1}$$

$\vec{c}$ is the connecting vector between the upstream and downstream SWORD nodes of the SWORD node closest to P_i. Then, the WSS $\tan\alpha$ can be calculated by dividing the fitted WSE difference by the length of the river section intersected by the beam ground track $\left(\|\vec{b}'\|\right)$ as follows:

$$\tan\alpha = \frac{\|\vec{b}\|\tan\beta}{\|\vec{b}'\|}\operatorname{sgn}\left(\vec{b}\cdot\vec{c}\right) \tag{2}$$

Note the multiplication by the sign of the scalar product of $\vec{b}$ and $\vec{c}$ in order to preserve the slope direction in the rare cases the river slope is negative. However, negative WSS results are rejected assuming outliers.

Using a Students t-distribution the WSS confidence interval (CI) is calculated at a 95% confidence level based on the standard error of the linear fitting of $\tan\beta$ (Niemeier, 2008). The CI is used as an outlier criteria to reject linear fits with high uncertainty. We use an angle-dependent outlier threshold $\mathrm{CI}_{th}(\gamma)$, which allows a higher CI for less orthogonal and thus longer intersections. At such intersections we assume a larger CI caused by small-scale WSS variations such as riffles and waves but better results than for shorter more orthogonal intersections with a possible lower CI. Additionally, the angle-dependent outlier threshold rejects any result from an intersection angle larger then the given maximum angle. $\mathrm{CI}_{th}(\gamma)$ is calculated as follows:

$$\mathrm{CI}_{th}(\gamma) = \begin{cases} \mathrm{CI}_{\max} - \dfrac{\mathrm{CI}_{\max}}{\gamma_{\max}}\gamma' & \text{if} \gamma' < \gamma_{\max} \\ 0, & \text{otherwise} \end{cases} \tag{3}$$

with

$$\gamma' = \begin{cases} 180° - \gamma & \text{if} \gamma > 90° \\ \gamma, & \text{otherwise} \end{cases} \tag{4}$$

and

$$\gamma = \arccos\frac{\vec{b}\cdot\vec{c}}{\|\vec{c}\|\|\vec{b}\|} \tag{5}$$

where γ is the intersection angle of the beam $\vec{b}$ with the reach centerline $\vec{c}$, $\mathrm{CI}_{\max}$ is the defined maximum CI parameter, and $\gamma_{\max}$ is the defined maximum intersection angle parameter. In this study, we use $\mathrm{CI}_{\max} = 300$ mm/km and $\gamma_{\max} = 65°$ as a result of empirical tests. Analogous to Section 3.2 and as shown in Figure 2 a weighted average is used to calculate time-variable mean values with daily temporal resolution where γ'^{-1} is used as weight. The median value of this time-variable WSS is used as an average reach scale along-track WSS.

3.4. Combined WSS Estimation

In order to increase the spatial and temporal coverage, we merge both, the across- and along-track methods, in one combined approach. This combination is necessary because depending on the intersection angle between the orbit ground track and the river centerline, it is possible that only one approach yields a WSS estimate. We expect the along-track method to yield results in situations where the across-track method can not be applied because of lacking simultaneous intersections with meridional reaches. On the other hand, orthogonal crossings with zonal reaches are favorable for the across-track approach, increasing the probability of multiple beams crossing the same reach. Therefore, the days of record in the WSS time series from both methods may differ.

As shown in Figure 2, the combination of both approaches is executed based on the time-variable WSS results with daily resolution. Because the across-track approach proves to be more accurate (see Section 4), its time series is used as the initial data. This time series is then supplemented by records from the along-track time series for dates on which no across-track observations are available. Thus, in the combined approach, the across-track WSS is used for each available day, while the along-track WSS is only used for days without across-track WSS. The average combined WSS is determined using the median of the combined time-variable WSS.

Table 1
Instantaneous Water Surface Slope Validation Results by Method and Used Beams With the Median Absolute Error (MAE), Coverage of the Studied Reaches, and Median 95% Confidence Interval (CI) of the Fitting

Method	Beams	n_{est}	n_{val}[a]	MAE $\left[\frac{mm}{km}\right]$	Coverage (%)	Med. CI $\left[\frac{mm}{km}\right]$
Across	All	18,178	20,021	24	82	
	Strong	4,889	5,345	23	78	
	Weak	4,382	4,839	23	75	
Along	All	4,455	4,645	57	78	30
	Strong	2,609	2,749	61	74	25
	Weak	1,846	1,896	52	62	36
Along[b]	All	12169	13183	133	96	79
	Strong	6,360	6,912	133	94	62
	Weak	5,809	6,271	134	94	110

[a]Estimates may be validated repeatedly when associated with multiple pairs of gauges. [b]Without outlier rejection.

4. Results and Discussion

We use two different methods to validate the WSS derived from ICESat-2 data. In Section 4.1, we compare the ICESat-2 WSS against time-variable in-situ WSS derived from two gauges enclosing the respective reach. The accuracy of the in-situ WSS depends on the gauge distance and river characteristics. We do not expect this data to reflect small-scale WSS variations between the gauges, but there is no more accurate time-variable WSS source covering large regions. As an alternative validation and to better quantify the quality of the ICESat-2 WSS, we apply the average combined WSS as a correction to water level time series from radar satellite altimetry in Section 4.2.

4.1. Validation Against Pairs of Gauges

To validate the method against in-situ WSS, we manually select pairs of in-situ gauges and determine their distance using the high-resolution SWORD centerline. We then calculate an in-situ WSS time series for each pair based on the difference between the two WSE time series. We apply our method to all SWORD reaches between the gauges of each pair and validate the instantaneous (Section 4.1.1), time-variable (Section 4.1.2), and average (Section 4.1.3) ICESat-2 WSS against the in-situ WSS time series, or the median in-situ WSS, respectively. The number of validation pairs is limited by the spatial distribution of the gauges, the epoch overlap with ICESat-2, and the availability of essential metadata such as the vertical datum, gauge zero, and exact location. We omit pairs of gauges with an average negative slope, mismatching vertical datums, or manually detected errors in the SWORD centerline between the gauges. In this way, 205 pairs of in-situ gauges are defined with 815 unique SWORD reaches located between the defined pairs. However, 132 reaches are located at the end and beginning of consecutive pairs of gauges, that is, within two validation sets, so there are more validation data than individual estimates. We manually select the pairs of gauges to ensure that they are connected without flow disturbances, that is, weirs, dams, or waterfalls.

4.1.1. Instantaneous WSS

Table 1 shows the results of the instantaneous WSS validated against the in-situ WSS. The median absolute error (MAE) refers to all validations, that is, if a reach is associated with multiple pairs of gauges, the WSS estimates are validated repeatedly. The along-track method is shown twice, with and without applying the angle-dependent outlier rejection. Each method is validated for strong and weak beams separately and with the data from all beams. Along-track results rejected as outliers because of a negative WSS fit are not listed in Table 1. Negative WSS fits occur for both beams with an equal probability of 35%. Table 1 also lists the percentage of the studied reaches covered by the respective method and subset of beams. Additionally, it shows the median CI for the along-track method.

Applying the across-track method to the data from all beams yields significantly more results than applying it to the strong or weak beams separately because there are more combinations possible between the intersections. Therefore, using all beams maximizes the coverage. However, the loss of coverage is not as significant as the loss of estimates when using only the strong or weak beams. Furthermore, the MAE is consistent at around 23 mm/km for any subset of beams with the across-track method. The MAE is significantly larger for the along-track method (57 mm/km), especially without the angle-dependent outlier rejection (133 mm/km). There is no difference in the MAE depending on the used beams with the along-track method. However, the CI is noticeably larger for the weak beams before outlier rejection. Figure 5 shows the absolute errors of the along-track method by the intersection angle and CI. Additionally, it shows the angle-dependent confidence threshold (black line) used for outlier rejection. Applying the outlier rejection to the results of the along-track method reduces the number of estimates by 63% and there are significantly fewer records than for the across-track method. Furthermore, the coverage of the studied reaches decreases, especially for the weak beams. However, the MAE improves by 57% with the application of the outlier rejection.

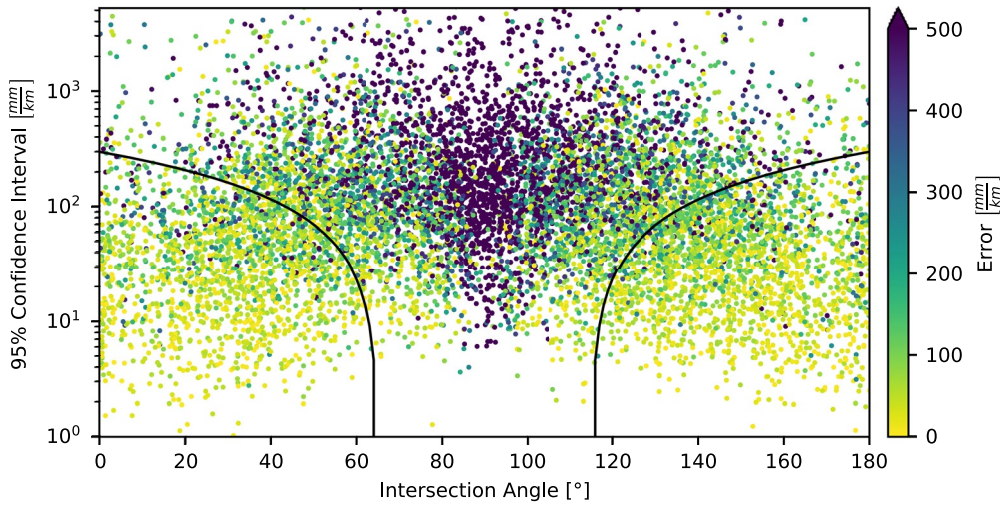

Figure 5. Along-Track water surface slope absolute errors by intersection angle and confidence interval with the applied angle-depended outlier threshold (black line). Estimates above the line are rejected.

Overall, the results in Table 1 show no notable difference in quality between the strong and weak beams throughout the methods, except for the number of estimates and coverage, which are higher for the strong beams. The covered percentage of the studied reaches is practically the same for both approaches, with 82% for the across-track method and 78% for the along-track method after the outlier rejection.

Figure 6 shows on the left the along-track WSS error by the length of the intersection between the satellite's ground track and the river surface area. The orange line shows the median error in a 200 m window. Additionally, the point color indicates the relative data point density. It shows a higher probability of large errors for shorter intersections. For intersections longer than 500 m, the rolling median along-track WSS error stays below 100 mm/km. The shortest intersection yielding a valid along-track WSS estimate is 66.2 m long. On the right, Figure 6 shows the across-track WSS error by the average width of the river reach according to SWORD data. The orange line shows the median error in a 100 m window. The narrowest river reach with an observed across-track WSS is 42 m wide. Although the probability of large errors rises with narrower reaches, the rolling median error stays below 55 mm/km.

As an example for fitting the along-track WSS and estimating the reference WSE for the across-track method, Figures 7–9 show selected intersection features with the Danube and Mississippi River. At the top, the figures show different types of outliers detected and rejected before the WSS estimation. The bottom plots show the along-track WSS fitted to the valid ATL13 observations and the elevation at the reference position (the

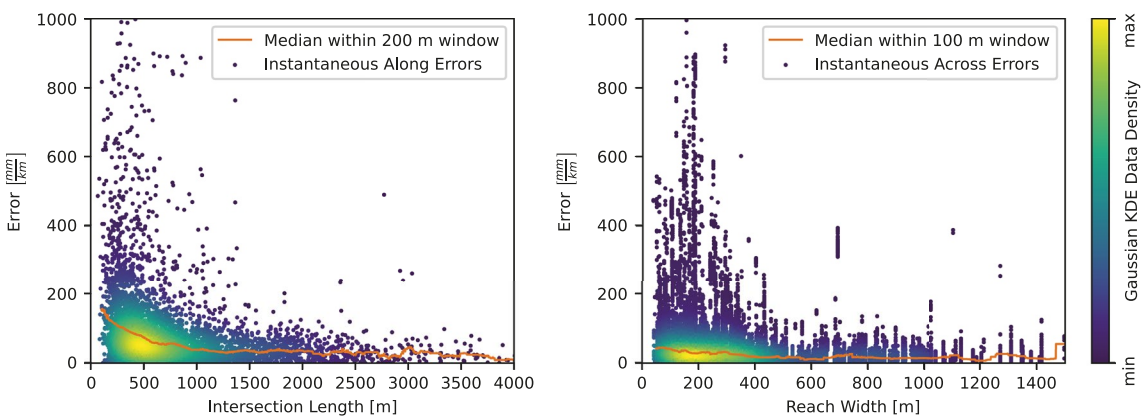

Figure 6. Left: Along-Track water surface slope (WSS) absolute errors by intersection length. Right: Across-Track WSS absolute errors by reach width. The orange lines show the rolling median within a 200 and 100 m window, respectively. The point color indicates the relative data point density.

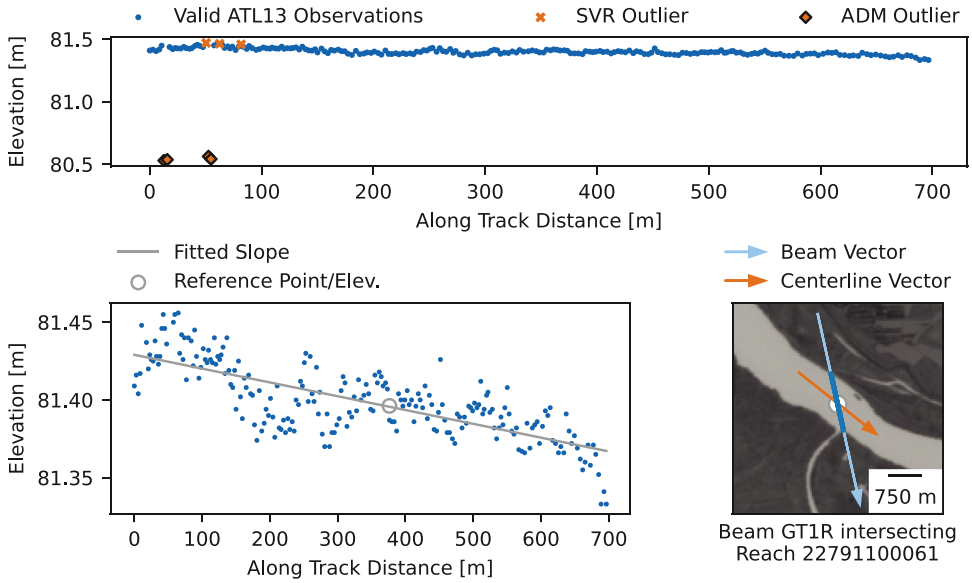

Figure 7. Beam GT1R (strong) intersecting reach 22791100061 (Danube) on 29 February 2020. Top: All ATL13 observations, including rejected outliers. Lower-left: Along-track Elevation of the ATL13 observations after outlier rejection with fitted along-track water surface slope (WSS) (89 mm/km, confidence interval: 10 mm/km). Lower-right: Beam GT1R intersecting the river centerline vector at an angle of 34° with ATL13 observations after outlier rejection. The resulting along-river WSS is 107 mm/km.

intersection with the centerline), which is used to calculate the across-track WSS in combination with simultaneous observations at other reference positions. The maps show the centerline and beam vector with the valid ATL13 observations and the feature reference location above a Sentinel-2 scene from the same month. The outliers in Figure 7 are caused by incorrect range measurements and detected by the ADM and SVR thresholds. The outliers in Figure 9 are caused by an additional intersection with the reach AOI. The WSE observations of the first intersection are considered outliers because the data is split into clusters at along-track gaps greater than 500 m and only the largest cluster is used. Figures 7 and 8 show the simultaneous intersection of the adjacent

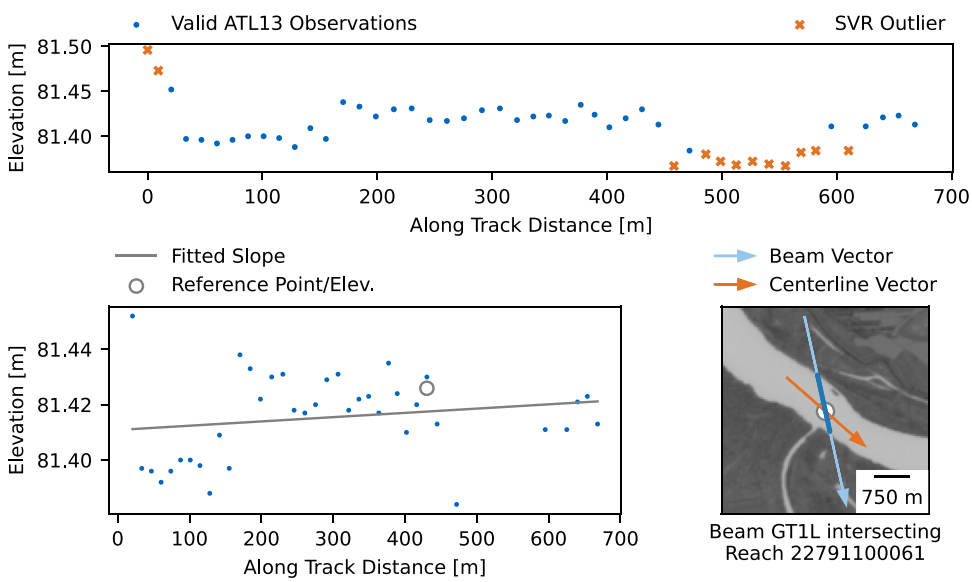

Figure 8. Lower-right: Beam GT1L (weak) intersecting reach 22791100061 (Danube) on 29 February 2020 at an angle of 32°. Top: ATL13 observations including outliers. Lower-left: water surface slope (WSS) fitted to valid ATL13 data. The resulting along-river WSS of −18 mm/km (confidence interval: 28 mm/km) is rejected.

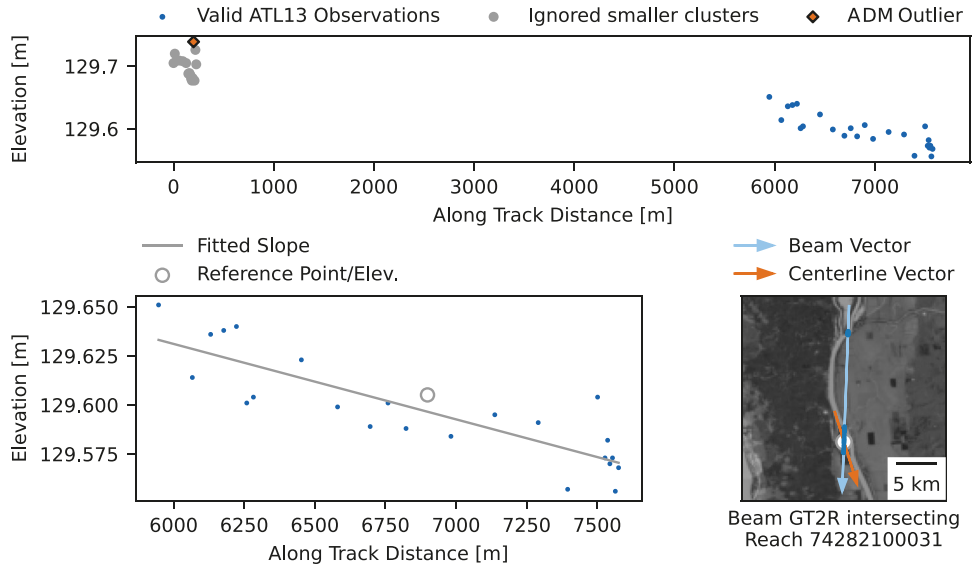

Figure 9. Lower-right: Beam GT2R (strong) intersecting reach 74282100031 (Mississippi) on 12 April 2020 at an angle of 19°. Top: ATL13 observations including outliers. Lower-left: water surface slope (WSS) fitted to valid ATL13 data. The resulting along-river WSS is 41 mm/km (confidence interval: 11 mm/km).

strong GT1R and weak GT1L beam with the same reach of the Danube River. There are significant less photon returns for the weak beam resulting in a lower spatial resolution of the ATL13 short segment data. Therefore, the WSS of −18 mm/km fitted to the weak data is not meaningful and gets rejected because it is negative. In contrast, the WSS fitting to the WSE of the strong beam is much more confident and accurate with a result of 107 mm/km while the in-situ WSS is 52 mm/km.

4.1.2. Time-Variable WSS

We do not distinguish between strong and weak beams for the time-variable WSS because the instantaneous WSS validation reveals no significant difference in quality (see Section 4.1.1). As mentioned in Sections 3.2 and 3.3, we use a weighted average to estimate time-variable WSS with daily temporal resolution using the WSE standard deviation or the intersection angle as the weight for the across- and along-track methods, respectively. Additionally, we combine both methods (Section 3.4) to increase the spatial and temporal resolution. Thus, there are three different WSS time series for each reach which we validate against the in-situ WSS. Table 2 shows the results of the validation.

There are 2,868 and 2,272 daily records for the across- and along-track methods. Combining both methods, we retrieve 3,671 estimates distributed over 726 reaches. 89% of the 815 studied reaches are covered by the combined approach, which is a 7% respectively 11% increase compared to using only the across- or along-track method (cf. Table 1). The median MAE slightly decreases by 2 mm/km for the across-track method using daily averages compared to the instantaneous results (cf. Table 1). For the along-track method, the MAE stays at 57 mm/km, and with 28 mm/km, the MAE of the combined time series is similar to the across-track method, which is plausible because the across-track method is preferred in the combination.

The temporal resolution of the combined WSS time series is sparse, with a maximum of 15 and a median of 5 records within the studied epoch from October 2018 to October 2021 because of the 91-day orbit repetition time. The median RMSE is 32, 80, and 49 mm/km for the across, along, and combined time series, and the median normalized RMSE (NRMSE) is 23%, 45%, and 35%, respectively. The mean in-situ WSS is used for the normalization of the RMSE. 79 reaches, about 10% of the studied reaches, do not have more than one daily WSS record. For the others, the median correlation coefficient is poor, especially for the combined method with only 0.35. Hence, even if the errors are small, the temporal variations are not well captured for most of the reaches. Therefore, the benefit of the daily WSS records is questionable or limited to individual reaches. On the other hand, local differences in WSS could cause the deviation of the ICESat-2 derived WSS over a relatively short baseline compared to the in-situ WSS measured along a much longer baseline.

Table 2
Time-Variable Water Surface Slope Validation Results Including the Absolute Error, Root Mean Square Error (RMSE), Normalized RMSE (NRMSE), Correlation Coefficient, and the Number of Records per Time Series

Measure	Method	Min	Mean	Med	Max	Std	n_{est}	n_{val}[a]
Abs. error[b] $\left[\frac{mm}{km}\right]$	Across	0	65	22	2,138	144	2,868	3,067
	Along	0	106	57	3,355	183	2,272	2,359
	Combined	0	75	28	3,267	158	3,671	3,886
RMSE[c] $\left[\frac{mm}{km}\right]$	Across	0	76	32	1,295	137	663	766
	Along	0	133	80	2,728	193	635	732
	Combined	0	98	49	2,728	177	726	841
NRMSE[c] (%)	Across	0	46	23	1,155	93	663	766
	Along	0	95	54	3,836	224	635	732
	Combined	0	68	35	3,836	198	726	841
Correlation[d]	Across	0.00	0.51	0.49	1.00	0.39	573	639
	Along	0.00	0.53	0.48	1.00	0.40	496	549
	Combined	0.00	0.44	0.35	1.00	0.38	647	729
Number of records[c]	Across	1	4	4	14	3	663	
	Along	1	4	3	12	2	635	
	Combined	1	5	5	15	3	726	

Note. The minimum, mean, median, maximum, and standard deviation values are given per quality measure and method.
[a]Estimations may be validated repeatedly when associated with multiple pairs of gauges. [b]Per record in all time series. [c]Per time series. [d]Per time series with more than one record.

Figure 10 shows selected good performing WSS time series estimated with the combined approach (blue) and the in-situ data (orange). The amplitude and temporal variability are well captured for the shown reaches, especially at the reaches of the rivers Loire and Ohio. Note, that the number of records varies per reach and the record interval is inconsistent within the time series. The interval is not necessarily coherent with the 91-day repeat orbit but can be lower when the reach is intersected by two ICESat-2 tracks (e.g., the shown reach of the Missouri River) or larger when there are outliers, no data due to cloud coverage, or the reach is only partially intersected by an ICESat-2 track.

4.1.3. Average WSS

We derive an average reach-scale WSS by calculating the median value of the daily WSS estimates. We compare this average WSS with the median of the in-situ WSS time series and the constant WSS provided with the SWORD data, which is derived from the MERIT Hydro DEM (see Section 2.2). Table 3 shows the MAE and coverage of the WSS from the three approaches and the SWORD WSS compared to the median in-situ WSS. The SWORD coverage is 100% because of the large swath width of the SRTM mission. However, the MAE of SWORD with 71 mm/km is more than three times larger than the MAE of the combined approach with 23 mm/km. Additionally, the histogram of the SWORD WSS in Figure 11 shows a tendency to values below 50 mm/km, which does not fit the distribution of the median in-situ WSS between the studied pairs of gauges. The different distributions of the in-situ WSS and the ICESat-2 or SWORD WSS might be biased because of the variable number of reaches between the pairs of gauges.

4.2. Correcting WSE Time Series From Radar Satellite Altimetry for WSS

To better quantify the quality of the ICESat-2 WSS, we apply the average combined WSS as a correction to DAHITI water level time series derived from satellite altimetry at 137 VS. As described in Section 2.4, the altimetry satellites do not cross a river precisely at the same position but within a range of approximately ±1 km. Combined with a meandering river, this range leads to a variation of river crossing positions of up to 5.7 km at the studied VS. Still, the observations of all orbit repetition cycles within this range are typically aggregated in one time series per VS. To apply the WSS to the DAHITI time series, we intersect the respective orbit of each time

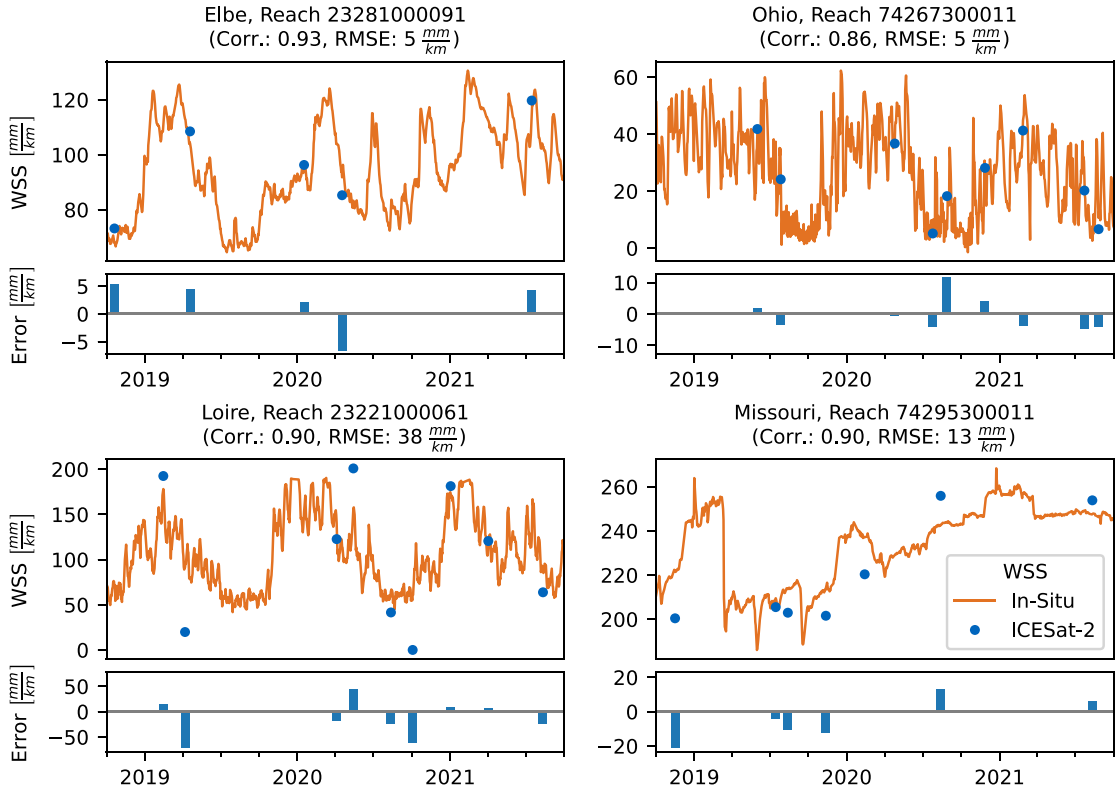

Figure 10. Water surface slope (WSS) time series for selected reaches of the rivers Elbe, Ohio, Loire, and Missouri. Blue dots show estimates using the combined approach. The in-situ WSS is shown in orange and the errors below. The correlation coefficient and root mean square error are given above each time series.

series record with the SWORD river centerline and determine the chainage of each intersection. By subtracting the VS reference point chainage, we get the crossing anomaly which is multiplied by the WSS to get the slope correction for each time series record. Outliers with errors above 75 cm in the DAHITI time series are removed before the comparison.

For this study, we select 137 VS from DAHITI. The VS must be adjacent to a gauge to validate the original DAHITI and WSS-corrected water level time series. Additionally, we selected only VS located between pairs of gauges so that we can compare the impact of the average ICESat-2 derived and SWORD WSS with the median in-situ WSS. We select only VS for which we can clearly and unambiguously determine the intersection of the orbits with the river centerline. For example, VS in curved reaches with multiple intersections and VS where the river runs nearly parallel to the satellite's ground track, which makes the exact measuring location hard to detect, are not part of this study. Furthermore, we do not use VS prone to the off-nadir effect caused by nearby water bodies because its errors likely exceed those caused by WSS. Tables B1 and B2 in the appendix list each studied VS with the mission, the reach, the amplitude of the crossing positions, the applied WSS, and the relative and absolute RMSE differences to the original DAHITI time series RMSE after applying the WSS as a correction. The relative RMSE difference is the percentage of the absolute RMSE difference from the RMSE before applying the correction.

Table 3
Coverage of the Studied Reaches and Median Absolute Errors (MAE) of the Average Reach-Scale Water Surface Slope (WSS) per Method and the SWORD WSS w.r.t. the Median In-Situ WSS

	MAE $\left[\frac{\text{mm}}{\text{km}}\right]$	Coverage [%]	n_{est}	n_{val}[a]
Across	19	81	663	780
Along	47	78	635	752
Combined	23	89	726	855
SWORD	71	100	811	943

[a]Estimates may be validated repeatedly when associated with multiple pairs of gauges.

Figure 12 shows histograms of the absolute and relative RMSE difference between the original DAHITI and the WSS-corrected time series for the in-situ, ICESat-2, and SWORD WSS. The RMSE improves by 30 cm or 66% in the best case. However, the histograms show only minor improvements for many VS and even an increased RMSE at some VS. For 88 VS (64% of the studied VS), the RMSE difference is insignificant between −2 and 2 cm using the WSS from ICESat-2. Overall, the correction based on the ICESat-2 WSS makes the most significant improvements with an RMSE difference below

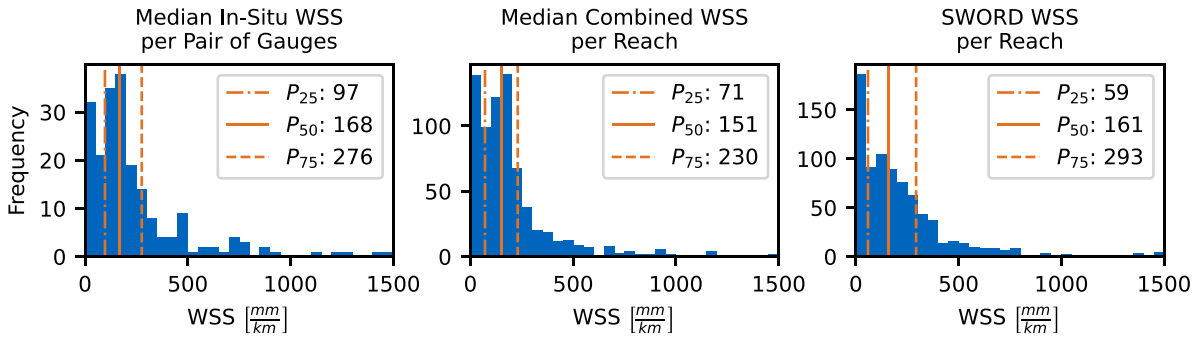

Figure 11. Histograms of the median in-situ water surface slope (WSS) per pair of gauges, the combined Ice, Cloud, and Land Elevation Satellite 2 WSS per reach, and the SWOT River Database WSS per reach.

−2 cm for 43 VS (31% of the studied VS) and a mean improvement of −2.20 cm RMSE (−8.24% NRMSE). The in-situ WSS performs similarly, with 44 VS (32% of the studied VS) improving by more than 2 cm and a mean improvement of −1.90 cm RMSE (−7.04% NRMSE). For some pairs of gauges used for validation, the SWORD connectivity differs from our manual determination. Therefore, a reduced set of results with only the stations between pairs of gauges connected according to SWORD is shown in orange in Figure 12. Even with the reduced set of VS, the WSS from ICESat-2 performs best. The correction based on the SWORD WSS has the lowest performance, with 37 VS (27% of the studied VS) improving by more than 2 cm and a mean improvement of −1.51 cm RMSE (−4.69% NRMSE). Using the SWORD WSS also results in the most considerable RMSE deterioration of +8 cm or +76%.

Figure 13 shows the absolute and relative RMSE differences after applying the WSS correction compared to the original DAHITI time series plotted depending on the reach WSS by source. The figure demonstrates, that most of the insignificant differences between −2 and 2 cm apparent in Figure 12 occur for VS in reaches of small WSS, shown in more detail in the plots on the right of Figure 13. The WSS correction's overall impact increases with a steeper WSS. However, there are VS where the RMSE increases or does not change significantly even in reaches with a steeper WSS. Since this occurs regardless of the used WSS source, either the reach-scale WSS is too coarse to reflect the local WSS, or the temporal WSS variability is so significant that an average WSS is not sufficient. With the ICESat-2 derived WSS correction, most degradations occur with WSS below 200 mm/km. However, for a WSS of more than 100 mm/km, the maximum RMSE improvements reach 5 cm or 30%. Although there are some outliers apparent, especially for the SWORD WSS, the majority of VS improves when correcting for WSS larger than 100 mm/km.

Figures 14 and 15 show, as an example, the original DAHITI and WSS-corrected water level time series at VS 37118 (Platte) and VS 13443 (Loire) compared to in-situ gauging data from USGS and Hydroportail, respectively. Both VS are derived from Sentinel-3A, and the combined WSS from this study is used for the WSS correction. The center plots show the crossing anomaly, that is, the difference of the nominal VS chainage to the chainage where the respective orbit crosses the river centerline. The bottom plots show the water level error w.r.t. the in-situ time series with and without the WSS correction. VS 37118 (Figure 14) shows a significant improvement in the time series, with the RMSE reduced by 29.39 cm or 65.82%. The combined WSS from this study used for correction is 1,164 mm/km, and the crossing anomaly magnitude is 1,545 m. At VS 13443 (Figure 15), the crossing anomaly magnitude is slightly larger (1,777 m), but the WSS of 430 mm/km used for correction is significantly lower than for VS 37118. Still, the RMSE improvements of 15.89 cm or 49.42% can be observed in the error bars and time series.

5. Conclusion

In this study, we successfully derive river WSS from ICESat-2 ATL13 observations at reach scale. The instantaneous results of the described methods, the across- and along-track approach, have median errors of 24 and 57 mm/km, respectively. We detect no difference in quality between WSS originating from strong or weak beam measurements. Only the confidence of fitting the along-track WSS is significantly lower for the weak beams. For the along-track approach, an angle-dependent outlier rejection is required, reducing the number of observations

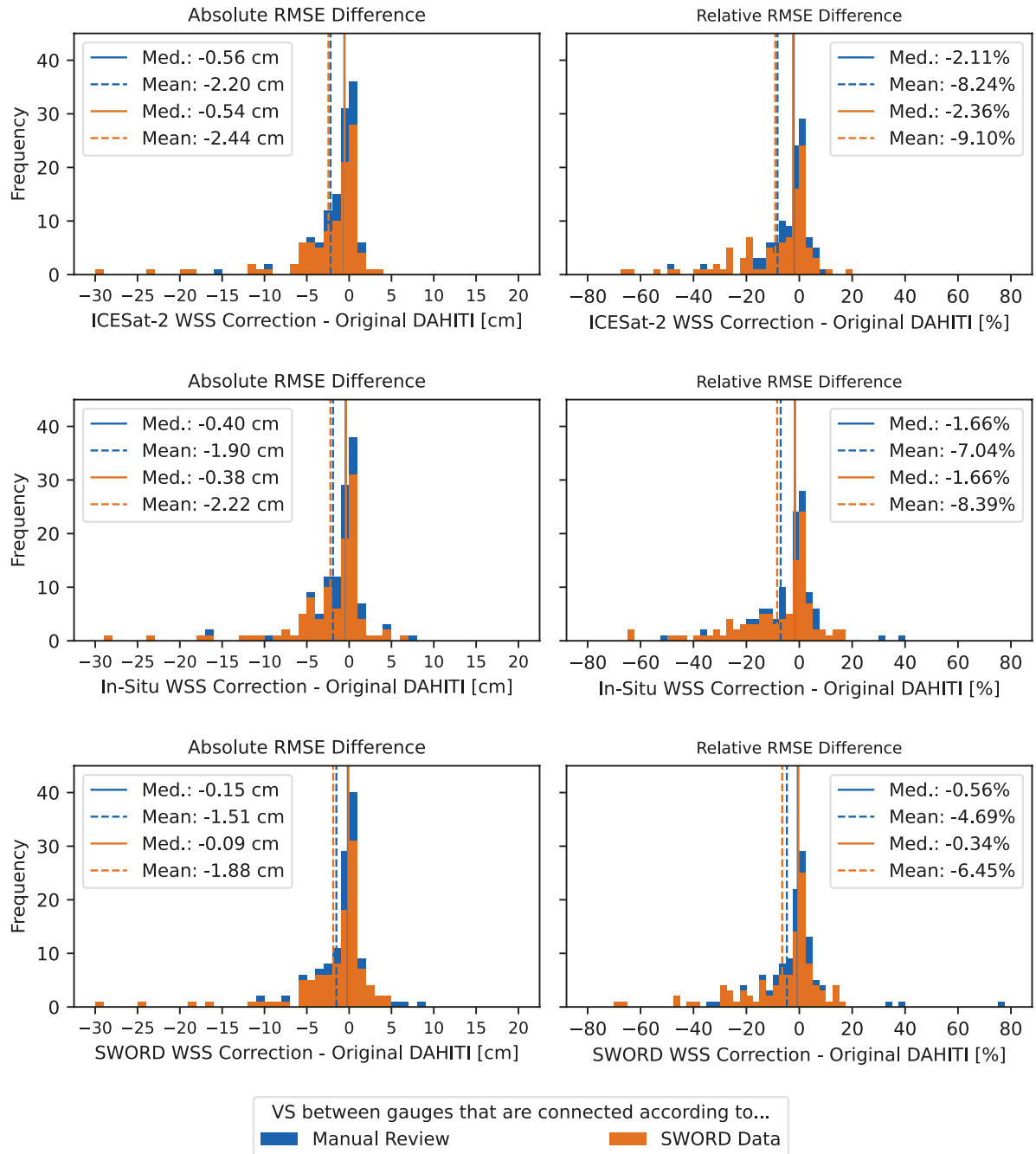

Figure 12. Histograms of the absolute (left) and relative (right) root mean square error difference applying the median combined (top), SWOT River Database (SWORD) (center), and median in-situ (bottom) water surface slope as a correction to the original Database for Hydrological Time Series of Inland Waters (DAHITI) water level time series. The in-situ histograms show all studied virtual stations in blue and a subset (orange) between pairs of gauges that are connected judging by SWORD data.

and coverage significantly but improving the estimated WSS quality. Overall, the across-track method has lower errors than the along-track method. The combined daily observations of both approaches cover 89% of the studied reaches with an MAE of 28 mm/km. However, the time variability of the WSS can not be estimated with confidence because although the median RMSE is low (49 mm/km), the median correlation coefficient of the time-variable WSS w.r.t. in-situ WSS between gauges is only 0.35. Additionally, the temporal resolution of the time-variable WSS is very sparse, with a median of only five records within the studied epoch of 2 years. Besides,

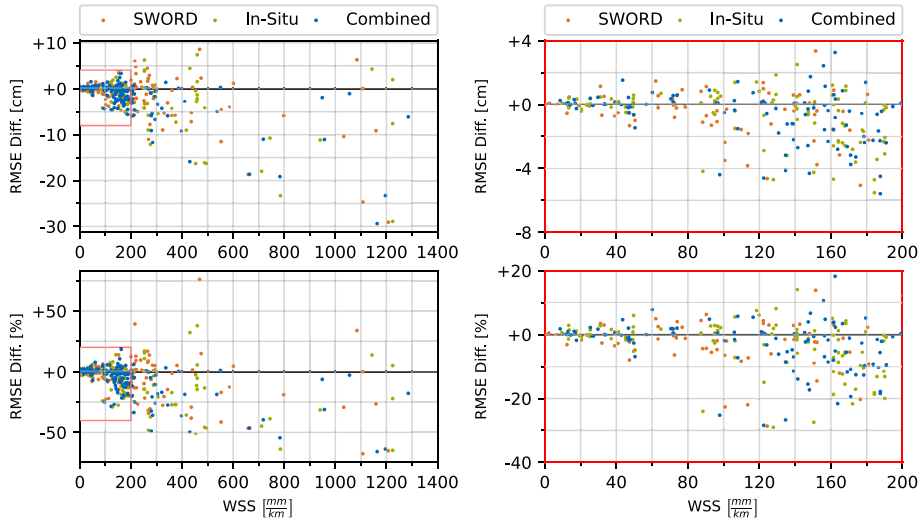

Figure 13. Root mean square error difference after applying the water surface slope (WSS)-correction compared to the original Database for Hydrological Time Series of Inland Waters time series for the 137 studied virtual stations. Negative values mean improvements due to the application of the WSS correction. The plots on the right show the regions of smaller WSS for more detail.

an average WSS is calculated for each reach also covering 89% of the reaches with an MAE of 23 mm/km w.r.t. average gauge data.

WSS can be an important correction for water level time series derived from radar satellite altimetry at VS when other errors like the off-nadir effect are not prevailing. To apply the WSS as a correction, the crossing chainage

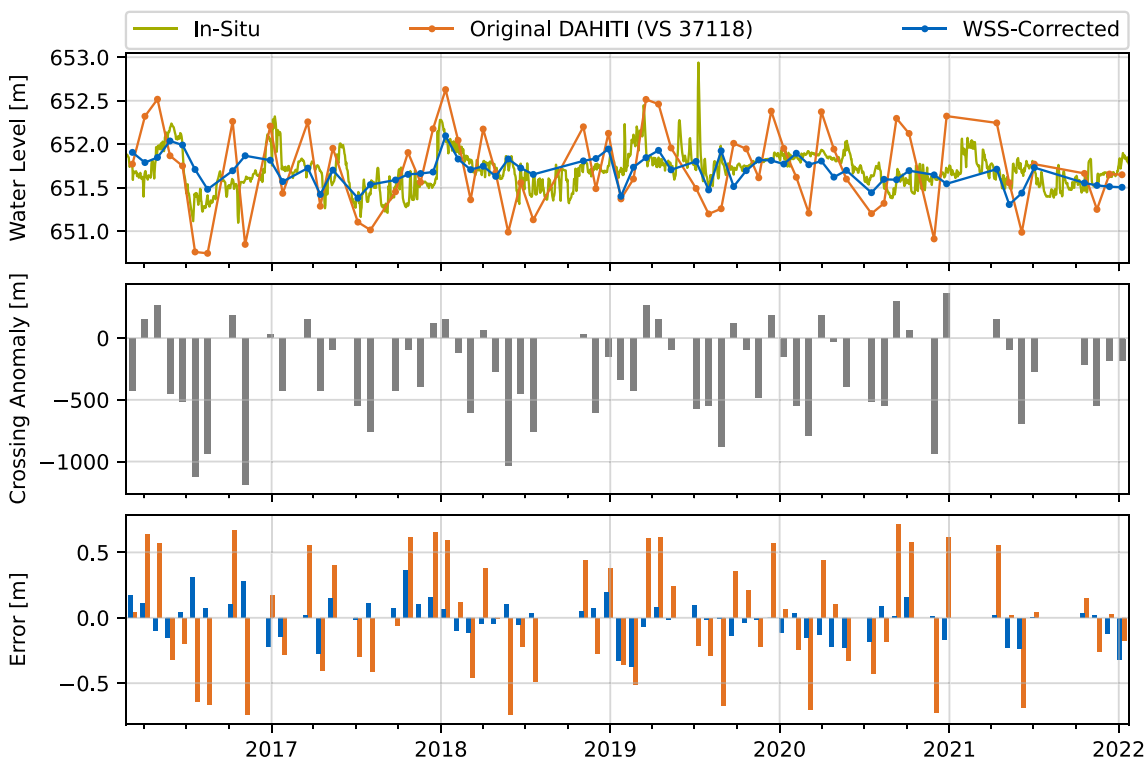

Figure 14. Top: Original Database for Hydrological Time Series of Inland Waters (DAHITI) and water surface slope (WSS)-corrected water level time series for virtual stations (VS) 37118 at the Platte River compared to the in-situ time series provided by U.S. Geological Survey (Station 06770200 near Kearney, Nebraska). Center: Crossing anomaly of the orbit ground tracks w.r.t. the VS nominal location. Bottom: Water level errors with and without the WSS correction applied.

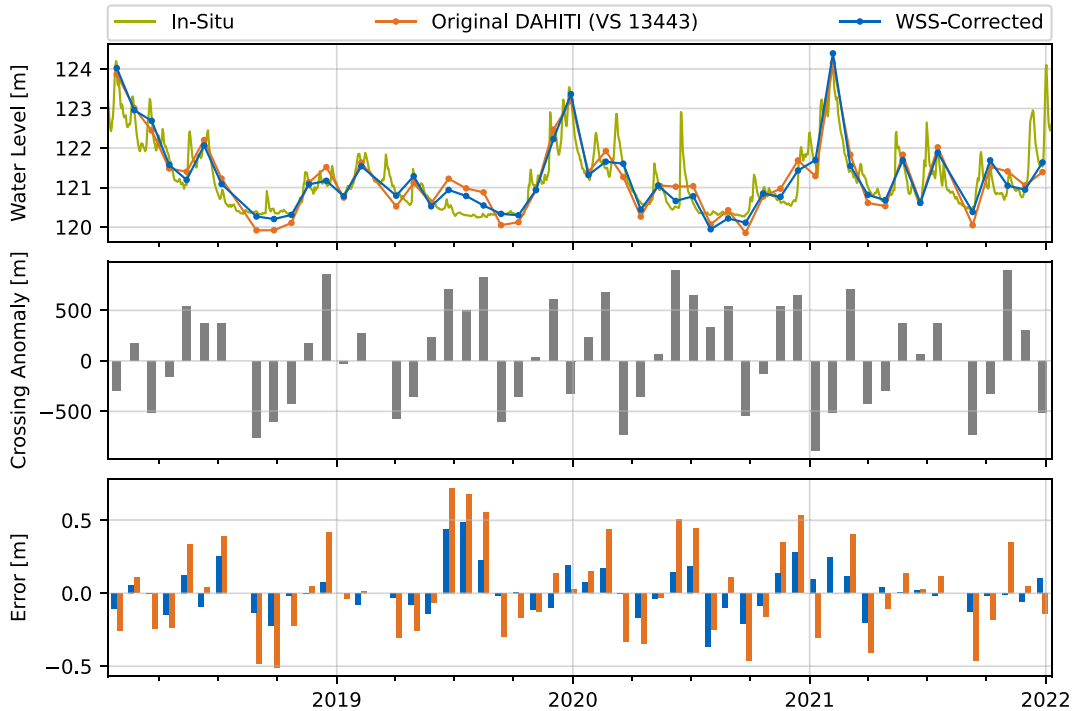

Figure 15. Top: Original Database for Hydrological Time Series of Inland Waters (DAHITI) and water surface slope (WSS)-corrected water level time series for virtual stations (VS) 13443 at the Loire River compared to the in-situ time series provided by Hydroportail (Station K418001010 at Gien). Center: Crossing anomaly of the orbit ground tracks w.r.t. the VS nominal location. Bottom: Water level errors with and without the WSS correction applied.

of the satellite orbit must be unambiguously determinable. Applying the WSS correction to the studied VS of the Sentinel-3A/B and Jason-2/3 missions improves the RMSE by up to 30 cm or 66%. However, the mean RMSE improvement is only 2.2 cm or 8.24% as for 64% of the studied VS, the impact is insignificant and sometimes leads to deterioration. A much more significant impact is expected for the calculation of reach-scale hydrographs of long repeat orbit missions like CryoSat-2, for which the WSS correction is mandatory because of the large crossing anomaly within the reach. Compared to using the ICESat-2 WSS from this study, the correction based on the SWORD WSS derived from DEM data has a lower impact, with a mean RMSE improvement of 1.51 cm or 4.69%. Overall, at VS situated in reaches with an average WSS below 100 mm/km, the WSS correction has no significant effect, presumably because the impact is lower than the radar altimeters accuracy. Still, a larger WSS should be considered an important source of error worth correcting, even with the less accurate WSS from SWORD.

The computational effort of the methodology to derive WSS from ICESat-2 is manageable, so the aim to apply the approach to all SWORD reaches globally is achievable. However, a denser cloud cover may affect observations of reaches in climate zones different from the studied area. Therefore, it must be determined whether the achieved coverage of 89% also applies globally.

Compared to the 91-day repeat orbit of ICESat-2, WSS time series derived from the upcoming SWOT mission will likely have a higher temporal resolution because the time interval of SWOT revisiting a reach is about 11 days due to its 120 km swath width and a 21-day repeat orbit (Biancamaria et al., 2016). Additionally, SWOT will use a Ka-band Radar Interferometer (KaRin) instrument, which can penetrate clouds in contrast to the ICESat-2 laser altimeter. Therefore, more data will be available for regions of high cloud coverage. SWOT is specifically designed to observe WSS and the science requirements of SWOT aim for a slope accuracy of 17 mm/km (Biancamaria et al., 2016), which would be better than the median results of this study. The airborne AirSWOT mission mounted with the same sensor as SWOT demonstrated that 90% of the slope errors were in the range of the required 17 mm/km with an MAE of 8.3 mm/km (Altenau et al., 2017). However, whether SWOT-derived WSS can match the accuracy of ICESat-2 with 23 mm/km must be studied after the launch of SWOT.

Appendix A: Studied Rivers With Characteristics and In-Situ Sourcess

Table A1 groups the studied rivers by the sources of in situ water level elevations used for validation. For each river, the characteristics are given according to the SWOT River Database (SWORD).

Table A1
Data Sources for the In-Situ Water Surface Elevation Data Used in This Study With the Median Width, Length, and Median Slope of the Studied River Sections According to SWOT River Database

In-situ source	River	Number of gauges	Median width (m)	Studied length (km)	Median Slope $\left[\frac{mm}{km}\right]$	Vertical datum
Bundesanstalt für Gewässerkunde (BfG)						Normalnull
	Elbe	15	171	591	201	
	Mosel	2	131	74	283	
	Neckar	2	107	33	218	
	Oder	3	174	44	309	
	Rhine	20	345	477	156	
U.S. Army Corps of Engineers (USACE)						NAVD88
	Mississippi	20	829	1,392	86	
U.S. Geological Survey (USGS)						NAVD88
	Allegheny	10	209	189	422	
	Altamaha	4	169	151	108	
	Arkansas	6	170	127	683	
	Big Sioux	4	45	127	184	
	Brazos	14	84	843	194	
	Cheyenne	5	51	200	928	
	Choctawhatchee	3	75	121	160	
	Colorado (Texas)	6	63	359	252	
	Illinois	9	277	178	12	
	Iowa	2	252	29	302	
	James	4	48	160	81	
	Kansas	6	179	161	332	
	Mississippi	12	829	1,392	86	
	Missouri	37	257	1,620	180	
	Neches	2	90	105	173	
	Ohio	12	685	392	25	
	Pascagoula	2	92	83	79	
	Platte	9	257	252	1,046	
	Red	11	155	809	210	
	Rock	7	160	178	157	
	Sabine	2	87	92	83	
	Trinity	9	80	330	134	
	Yellowstone	3	313	33	198	
Republic Hydrometeorological Service of Serbia (HIDMET)						Adriatic
	Danube	11	664	348	7	
Hydroportail						IGN 1969

Table A1
Continued

In-situ source	River	Number of gauges	Median width (m)	Studied length (km)	Median Slope $\left[\frac{mm}{km}\right]$	Vertical datum
	Garonne	4	184	113	289	
	Loire	17	318	476	310	
	Saône	4	234	59	21	

Appendix B: Detailed Results of the VS Water Surface Slope (WSS) Correction

Tables B1 and B2 list the WSS-corrected results for each studied virtual station (VS) and WSS source in Europe and North America, respectively.

Table B1
Results of the WSS Correction for Virtual Stations in Europe

				WSS $\left[\frac{mm}{km}\right]$			Rel. RMSE difference (%)			Abs. RMSE difference (cm)		
River VS ID	Mis.	Reach ID	Crossing ampl. (m)	1	2	3	1	2	3	1	2	3
Danube												
14383	S3A	22737900241	2,017	13	1	10	+0.99	+0.09	+0.67	+0.12	+0.01	+0.08
17612	S3B	22737900251	1,770	9	2	13	+1.79	+0.49	+2.91	+0.25	+0.07	+0.41
15558	S3B	22737900271	2,262	18	0	13	−1.79	+0.00	−1.41	−0.26	+0.00	−0.20
17227	S3B	22750000011	1,146	25	33	31	+2.23	+2.99	+2.78	+0.38	+0.51	+0.47
17970	S3A	22770000021	1,685	47	63	37	+2.03	+2.51	+1.62	+0.44	+0.55	+0.35
15195	S3B	22770000021	1,401	47	63	37	−1.36	−1.35	−1.28	−0.20	−0.20	−0.19
16850	S3B	22770000081	1,614	60	0	50	+7.77	+0.00	+6.00	+0.75	+0.00	+0.58
21581	S3A	22770000141	1,634		73	50		−6.38	−5.21		−0.80	−0.65
18403	S3A	22770000221	1,740	48	0	49	−1.55	+0.00	−1.50	−0.19	+0.00	−0.18
17363	S3B	22770000231	1,992	43	215	49	−0.19	+39.36	+0.85	−0.03	+5.96	+0.13
17364	S3B	22791100061	1,117	47	74	45	−0.89	−1.04	−0.87	−0.18	−0.21	−0.18
16479	S3B	22791100071	1,484	47	0	45	−1.75	+0.00	−1.66	−0.51	+0.00	−0.49
Elbe												
13618	S3A	23281000071	1,649	17	74	50	+0.56	+4.03	+2.42	+0.08	+0.61	+0.37
13631	S3B	23281000111	2,398	122	124	128	−28.40	−28.64	−29.03	−4.60	−4.64	−4.70
13619	S3A	23281000141	1,933	121	200	128	+0.91	+12.24	+1.93	+0.13	+1.80	+0.28
13620	S3A	23281000151	2,023	145	213	141	+0.67	+6.64	+0.49	+0.11	+1.04	+0.08
13621	S3B	23281000171	1,222	147	79	141	−1.75	−1.19	−1.63	−0.27	−0.19	−0.26
13627	S3A	23283000041	1,784	164	0	172	−21.61	−0.00	−21.66	−2.80	−0.00	−2.80
13626	J23	23283000081	1,565	200	222	204	+0.97	+1.64	+1.08	+0.20	+0.35	+0.23
13623	S3A	23283000091	1,611	178	221	190	−12.63	−13.18	−13.12	−2.00	−2.09	−2.08
13630	S3A	23285000011	1,587	204	475	190	−20.11	+14.97	−19.98	−3.11	+2.32	−3.09
13632	J23	23285000021	1,372	213	260	212	−4.74	−5.00	−4.73	−1.14	−1.20	−1.14
13635	S3B	23285000091	1,406	216	227	212	−25.14	−26.59	−24.56	−4.72	−4.99	−4.61
13634	S3A	23285000101	2,524	211	12	212	−33.54	−3.17	−33.53	−5.75	−0.54	−5.75
13649	J23	23285000141	1,071	188	441	204	−2.11	+1.45	−2.18	−0.43	+0.29	−0.44
13650	S3A	23285000161	1,909	298	127	289	−2.78	−6.03	−3.39	−0.56	−1.21	−0.68
13651	S3A	23285000181	1,000	296	202	289	−10.54	−8.38	−10.40	−1.76	−1.40	−1.74

Table B1
Continued

River VS ID	Mis.	Reach ID	Crossing ampl. (m)	WSS [mm/km] 1	WSS [mm/km] 2	WSS [mm/km] 3	Rel. RMSE difference (%) 1	Rel. RMSE difference (%) 2	Rel. RMSE difference (%) 3	Abs. RMSE difference (cm) 1	Abs. RMSE difference (cm) 2	Abs. RMSE difference (cm) 3
13652	S3B	23285000211	1,410	304	110	264	−18.07	−8.36	−17.19	−3.38	−1.56	−3.22
13653	S3A	23285000241	1,409	124	251	256	−3.23	+0.55	+0.85	−0.57	+0.10	+0.15
Loire												
13412	S3A	23221000171	1,728	174	165	186	−12.55	−12.06	−13.13	−3.28	−3.16	−3.43
13417	S3B	23227000021	1,605	321	32	360	−16.91	−2.65	−17.21	−4.25	−0.67	−4.32
13415	S3A	23227000031	1,499	344	373	360	−27.39	−27.09	−27.29	−5.88	−5.82	−5.86
13419	S3B	23227000061	2,288	536	553	376	−18.65	−17.00	−27.13	−5.00	−4.56	−7.28
13420	S3A	23227000091	1,532	205	284	431	−4.66	+5.33	+32.31	−0.64	+0.73	+4.44
13421	S3A	23227000151	1,879	398	274	417	−36.29	−30.59	−35.60	−9.21	−7.77	−9.04
13443	S3A	23227000181	1,777	430	269	453	−49.42	−34.22	−50.73	−15.89	−11.00	−16.31
13399	J23	23227000191	732	276	1,084	453	−4.91	+33.92	−2.46	−0.91	+6.30	−0.46
13578	S3A	23227000251	1,268	411	254	459	−18.69	−21.61	−14.54	−2.85	−3.29	−2.22
Oder												
13660	S3A	24222100071	1,889	279	436	267	−48.60	−38.18	−47.94	−9.12	−7.17	−9.00
13661	S3A	24222100071	1,790	279	436	267	−32.36	−29.14	−31.79	−5.86	−5.28	−5.76
18752	S3A	24222100081	1,790	270	295	267	−0.10	+5.08	−0.68	−0.02	+0.80	−0.11
18753	S3A	24222300011	3,687	285	324	276	−35.81	−27.61	−37.18	−11.67	−9.00	−12.11
Rhine												
13593	S3A	23261000141	1,842	195	242	191	−0.67	+1.36	−0.82	−0.16	+0.32	−0.19
13584	S3A	23261001811	1,428	123	20	127	+0.18	−0.14	+0.23	+0.08	−0.06	+0.10
13654	J23	23263000081	954	71	71	93	+1.86	+1.89	+2.70	+0.35	+0.36	+0.51

Note. 1: Combined WSS from this study, 2: SWORD WSS, 3: In-Situ WSS. SWORD, SWOT River Database; RMSE, root mean square error; WSS, water surface slope; VS, virtual stations.

Table B2
Results of the WSS Correction for Virtual Stations in North America

River VS ID	Mis.	Reach ID	Crossing ampl. (m)	WSS [mm/km] 1	WSS [mm/km] 2	WSS [mm/km] 3	Rel. RMSE difference (%) 1	Rel. RMSE difference (%) 2	Rel. RMSE difference (%) 3	Abs. RMSE difference (cm) 1	Abs. RMSE difference (cm) 2	Abs. RMSE difference (cm) 3
Illinois												
15094	S3A	74282100021	2,841	44	31	14	+4.65	+3.47	+1.44	+1.52	+1.14	+0.47
14256	S3A	74282100071	2,573	16	62	18	+1.05	+4.98	+1.15	+0.31	+1.47	+0.34
18655	S3A	74282700071	1,541	27	143	25	−0.49	+3.25	−0.62	−0.09	+0.60	−0.12
Mississippi												
11484	J23	74210000281	2,677	34	72	95	−0.06	+0.18	+0.48	−0.03	+0.08	+0.22
13250	S3B	74230300051	1,816	39	0	41	+0.78	−0.00	+0.86	+0.16	−0.00	+0.18
17172	S3B	74255000021	1,213	57	266	87	+0.02	+7.78	+0.50	+0.00	+1.67	+0.11
22858	S3A	74255000071	2,108	100	139	94	−1.93	−1.56	−1.91	−0.52	−0.42	−0.52
15411	S3B	74257000021	4,936	50	151	98	−2.65	+13.87	+2.17	−0.64	+3.35	+0.52
15412	S3B	74257000031	2,374	106	148	95	−1.49	+0.39	−2.61	−0.35	+0.09	−0.62
36325	S3A	74259000021	2,668	72	122	95	+0.51	+0.67	+0.49	+0.17	+0.22	+0.16

Table B2
Continued

River VS ID	Mis.	Reach ID	Crossing ampl. (m)	WSS $\left[\frac{mm}{km}\right]$			Rel. RMSE difference (%)			Abs. RMSE difference (cm)		
				1	2	3	1	2	3	1	2	3
14252	S3A	74259000021	1,984	72	122	95	+1.77	+4.35	+2.83	+0.56	+1.37	+0.89
15776	S3B	74270100131	1,771	129	140	106	−1.19	−0.56	−1.96	−0.25	−0.11	−0.40
15777	S3B	74270500021	2,464	108	39	106	+5.74	+0.43	+5.54	+1.43	+0.11	+1.38
17170	S3B	74270500021	1,393	108	39	106	−7.26	−3.51	−7.18	−1.51	−0.73	−1.49
14253	S3A	74270700061	1,929	97	139	97	+0.47	+2.87	+0.47	+0.10	+0.60	+0.10
16793	S3B	74270700221	2,306	72	162	97	+0.46	+3.02	+1.29	+0.14	+0.90	+0.38
14254	S3A	74270900021	1,443	74	122	97	+2.02	+3.49	+2.66	+0.57	+0.99	+0.76
16794	S3B	74270900031	5,748	98	113	88	−25.22	−21.96	−24.02	−4.39	−3.82	−4.18
36755	S3B	74289500091	1,704	386	361	459	+0.35	−1.22	+5.63	+0.09	−0.33	+1.53
22867	S3A	74289500101	1,555	550	601	459	+1.07	+4.60	−5.29	+0.27	+1.18	−1.36
18656	S3A	74289500131	2,287	141	301	459	−13.89	−0.06	+37.94	−2.70	−0.01	+7.39
Missouri												
15096	S3A	74291100171	1,554	210	469	179	+5.67	+76.12	+0.96	+0.64	+8.58	+0.11
19674	S3B	74291100241	1,578	187	279	178	−10.23	−6.26	−10.45	−1.65	−1.01	−1.69
22888	S3A	74291100281	1,870	179	114	177	−9.58	−7.30	−9.54	−2.38	−1.82	−2.37
14790	S3A	74291300011	1,754	169	213	161	−11.68	−13.22	−11.51	−2.63	−2.98	−2.59
17590	S3B	74291300061	1,804	156	96	161	−0.37	−1.91	−0.17	−0.08	−0.40	−0.03
36834	J23	74291300061	1,346	156	96	161	−6.93	−4.70	−7.07	−1.57	−1.07	−1.60
22889	S3B	74291500021	1,369	148	176	161	−17.28	−20.28	−18.72	−4.31	−5.06	−4.67
22890	S3A	74291500031	2,199	169	93	168	−5.51	−5.56	−5.55	−1.29	−1.30	−1.30
14470	S3A	74291500061	1,752	147	47	168	−15.49	−7.97	−15.50	−2.57	−1.32	−2.57
36891	J23	74291500061	1,565	136	47	168	−5.36	−2.31	−5.90	−1.22	−0.53	−1.34
17213	S3B	74291500141	1,419	162	238	161	+3.88	+9.66	+3.73	+0.61	+1.53	+0.59
15649	S3B	74291700011	1,617	162	41	161	−7.96	−2.71	−7.95	−1.56	−0.53	−1.56
17214	S3B	74291700041	1,899	157	125	161	+4.79	+2.99	+5.09	+1.14	+0.71	+1.21
14151	S3A	74291900031	2,544	179	19	168	+5.17	−0.32	+4.30	+1.39	−0.09	+1.15
18020	S3A	74291900041	1,708	167	267	168	+3.44	+8.84	+3.52	+0.86	+2.21	+0.88
15283	S3B	74291900091	1,668	139	288	166	−11.34	−11.07	−12.33	−2.21	−2.16	−2.40
16835	S3B	74291900091	1,700	139	288	166	−6.95	+0.81	−6.65	−1.23	+0.14	−1.17
22891	S3A	74291900121	1,807	162	102	151	+2.30	−1.99	+1.19	+0.35	−0.30	+0.18
18661	S3A	74291900131	2,498	138	88	151	−4.76	−4.40	−4.61	−1.20	−1.11	−1.16
16456	S3B	74293300021	4,395	188	206	184	−17.82	−12.02	−18.69	−4.49	−3.03	−4.71
17455	S3B	74293300021	1,465	188	206	184	−18.41	−19.59	−18.19	−5.58	−5.94	−5.52
37033	J23	74293300041	1,222	184	181	457	−9.15	−9.11	−11.34	−2.24	−2.23	−2.78
22892	S3A	74293300071	1,772	177	205	123	−2.61	−2.05	−3.14	−0.57	−0.45	−0.69
16457	S3B	74293300101	1,918	171	0	123	−19.40	+0.00	−14.92	−3.75	+0.00	−2.89
22894	S3A	74293300131	1,521	199	134	190	+0.19	−1.47	−0.20	+0.04	−0.29	−0.04
22895	S3B	74293500011	1,912	203	50	190	−11.42	−4.84	−11.38	−2.33	−0.99	−2.33
22896	S3B	74293700011	1,628	202	152	190	−1.45	−2.39	−2.01	−0.24	−0.40	−0.34
19675	S3A	74293700061	2,416	191	151	21	−9.30	−8.85	−1.71	−2.39	−2.28	−0.44
18662	S3A	74293700081	2,055	186	250	21	−1.51	+0.17	−0.74	−0.61	+0.07	−0.30
38434	S3A	74295100031	2,501	135	101	150	−26.70	−22.63	−27.44	−4.13	−3.50	−4.25

Table B2
Continued

River VS ID	Mis.	Reach ID	Crossing ampl. (m)	WSS $\left[\frac{mm}{km}\right]$			Rel. RMSE difference (%)			Abs. RMSE difference (cm)		
				1	2	3	1	2	3	1	2	3
22897	S3B	74295100031	1,026	135	101	135	−8.61	−6.44	−8.66	−3.17	−2.37	−3.19
14950	S3A	74297700211	2,282	92	87	118	+4.83	+4.42	+7.52	+0.90	+0.83	+1.41
16234	S3B	74297700251	1,794	116	72	120	+5.44	−0.34	+6.09	+0.74	−0.05	+0.83
18664	S3A	74299300181	2,006	162	90	141	−5.11	−4.30	−5.79	−0.83	−0.69	−0.94
14413	S3A	74299300181	2,333	162	90	141	+18.25	+6.29	+14.02	+3.26	+1.12	+2.50
19687	S3A	74299900021	2,096	664	659	711	−46.40	−46.53	−44.80	−18.63	−18.68	−17.99
22909	S3A	74299900041	1,938	949	798	1,144	−6.26	−18.86	+13.78	−1.95	−5.86	+4.28
Ohio												
14904	S3A	74265000091	1,687	14	0	24	−0.14	+0.00	−0.21	−0.05	+0.00	−0.08
36357	J23	74265000091	1,602	14	0	24	+0.01	+0.00	+0.03	+0.01	+0.00	+0.01
16549	S3B	74267100061	1,741	12	77	65	+0.15	+2.30	+1.73	+0.06	+0.93	+0.70
15867	S3B	74267700151	1,913	30	0	25	+1.70	+0.00	+1.49	+0.46	+0.00	+0.40
36420	J23	74267700161	1,418	34	13	25	+0.10	+0.03	+0.07	+0.04	+0.01	+0.03
36421	S3A	74267700161	1,571	34	13	25	−0.06	−0.06	−0.07	−0.02	−0.02	−0.02
Platte												
37079	J23	74294100031	2,050	718	553	744	−39.59	−41.46	−38.70	−11.00	−11.51	−10.75
37089	J23	74294300041	1,264	957	1,033	941	−31.12	−29.21	−31.46	−11.07	−10.39	−11.18
15689	S3B	74294500011	1,091	1,196	1,108	785	−63.72	−67.53	−63.79	−23.29	−24.68	−23.31
37117	S3A	74294500211	1,814	1,286	1,159	1,225	−17.77	−26.56	−22.09	−6.12	−9.15	−7.61
37118	S3A	74294500221	1,545	1,164	1,207	1,225	−65.82	−65.12	−64.75	−29.39	−29.08	−28.91
37120	J23	74294500231	1,530	1,055	1,108	1,225	−2.77	+0.08	+5.11	−1.07	+0.03	+1.98
Red												
35699	S3B	74223700061	1,570	147	272	129	+3.97	+13.77	+2.97	+0.84	+2.91	+0.63
35705	S3B	74223700081	2,054	156	0	129	+10.62	+0.00	+8.13	+2.43	+0.00	+1.86
35708	S3B	74223900031	3,045	150	216	141	−0.59	+1.84	−0.85	−0.21	+0.66	−0.30
35713	S3B	74223900051	1,650	106	7	141	+0.79	+0.04	+1.61	+0.24	+0.01	+0.50
35720	S3B	74225000031	1,652	131	171	177	−6.13	−5.51	−5.49	−1.78	−1.60	−1.60
35722	S3A	74225000051	1,825	170	167	147	−1.12	−1.14	−1.23	−0.42	−0.42	−0.46
35730	S3A	74225000091	1,995	146	151	147	−2.30	−2.29	−2.30	−0.63	−0.63	−0.63
35741	S3A	74225000151	1,606	140	180	164	+0.30	+2.31	+1.23	+0.08	+0.63	+0.34
35742	S3B	74225000161	1,897	187	211	164	−5.63	−5.45	−5.63	−2.27	−2.20	−2.27
35752	S3A	74225000201	1,644	158	251	164	−8.55	−9.78	−8.67	−2.31	−2.65	−2.35
35750	S3B	74225000201	1,507	158	251	164	−1.66	+0.52	−1.59	−0.39	+0.12	−0.38
35751	J23	74225000201	1,941	171	251	253	−10.83	−14.33	−14.39	−3.17	−4.19	−4.21
35757	S3A	74225000241	1,678	263	212	253	+0.64	−0.51	+0.36	+0.19	−0.15	+0.11
35759	S3B	74225000251	1,535	149	265	253	+6.70	+16.92	+15.57	+1.74	+4.40	+4.05
35764	S3B	74225000301	1,556		219	253		+9.26	+10.85		+3.28	+3.84
35763	S3A	74225000301	2,947		219	253		+12.83	+17.04		+4.70	+6.24
35779	S3B	74227100161	1,486	294	152	294	−25.73	−14.51	−25.73	−6.67	−3.76	−6.67
35781	S3A	74227100171	1,867	336	380	294	+3.25	+5.20	+1.70	+1.39	+2.21	+0.72
35783	S3A	74227100221	2,195	282	329	306	−20.70	−20.38	−20.79	−5.37	−5.29	−5.40
35796	J23	74227700011	1,465		584	488		−12.73	−13.31		−4.02	−4.20

Table B2
Continued

River VS ID	Mis.	Reach ID	Crossing ampl. (m)	WSS $\left[\frac{mm}{km}\right]$ 1	WSS 2	WSS 3	Rel. RMSE difference (%) 1	Rel. RMSE difference (%) 2	Rel. RMSE difference (%) 3	Abs. RMSE difference (cm) 1	Abs. RMSE difference (cm) 2	Abs. RMSE difference (cm) 3
35797	S3A	74227700021	1,617	783	495	488	−54.40	−46.27	−45.82	−19.14	−16.28	−16.12
Yellowstone												
38432	S3A	74298100021	1,828	50	343	174	−6.91	−14.61	−17.10	−1.46	−3.08	−3.60

Note. 1: Combined WSS from this study, 2: SWORD WSS, 3: In-Situ WSS. SWORD, SWOT River Database; RMSE, root mean square error; WSS, water surface slope; VS, virtual stations.

Data Availability Statement

The results of this study are available at Zenodo via https://doi.org/10.5281/zenodo.7098114. The ICESat-2 ATL13 data used for the WSS estimation in the study are available at the National Snow & Ice Datacenter (NSIDC) via https://doi.org/10.5067/ATLAS/ATL13.005 (Jasinski et al., 2021b). The SWOT River Database (SWORD) (Version v1) used for the reach definition and centerlines in the study are available at Zenodo via https://doi.org/10.5281/zenodo.4917236 (Altenau et al., 2021b). The water level time series from the Database for Hydrological Time Series of Inland Waters (DAHITI) used to assess the impact of correcting virtual stations for water surface slope are available at https://dahiti.dgfi.tum.de (Schwatke et al., 2015).

Acknowledgments
This work was funded by the Deutsche Forschungsgemeinschaft (DFG, German Research Foundation)—Project number 324641997, Grant DE 2174/10-2. Open access funding enabled and organized by Projekt DEAL. We thank the Wasserstraßen- und Schifffahrtsverwaltung des Bundes (WSV), Bundesanstalt für Gewässerkunde (BfG), U.S. Army Corps of Engineering (USACE), U.S. Geological Survey (USGS), Hydroportail, and the Republic Hydrometeorological Service of Serbia (HIDMET) for providing the in-situ data.

References

Allen, G. H., & Pavelsky, T. (2018). Global extent of rivers and streams. *Science*, *361*(6402), 585–588. https://doi.org/10.1126/science.aat0636

Altenau, E. H., Pavelsky, T. M., Durand, M. T., Yang, X., Frasson, R. P. D. M., & Bendezu, L. (2021a). The Surface Water and Ocean Topography (SWOT) Mission River Database (SWORD): A global river network for satellite data products. *Water Resources Research*, *57*(7), e2021WR030054. https://doi.org/10.1029/2021WR030054

Altenau, E. H., Pavelsky, T. M., Durand, M. T., Yang, X., Frasson, R. P. D. M., & Bendezu, L. (2021b). SWOT River Database (SWORD) (version v1) [Dataset]. Zenodo. https://doi.org/10.5281/zenodo.4917236

Altenau, E. H., Pavelsky, T. M., Moller, D., Lion, C., Pitcher, L. H., Allen, G. H., et al. (2017). AirSWOT measurements of river water surface elevation and slope: Tanana River, AK. *Geophysical Research Letters*, *44*(1), 181–189. https://doi.org/10.1002/2016GL071577

Biancamaria, S., Lettenmaier, D. P., & Pavelsky, T. M. (2016). The SWOT mission and its capabilities for land hydrology. *Surveys in Geophysics*, *37*(2), 307–337. https://doi.org/10.1007/s10712-015-9346-y

Bjerklie, D. M., Birkett, C. M., Jones, J. W., Carabajal, C., Rover, J. A., Fulton, J. W., & Garambois, P.-A. (2018). Satellite remote sensing estimation of river discharge: Application to the Yukon River Alaska. *Journal of Hydrology*, *561*, 1000–1018. https://doi.org/10.1016/j.jhydrol.2018.04.005

Boergens, E., Dettmering, D., Schwatke, C., & Seitz, F. (2016). Treating the hooking effect in satellite altimetry data: A case study along the Mekong River and its tributaries. *Remote Sensing*, *8*(2), 91. https://doi.org/10.3390/rs8020091

Boergens, E., Schmidt, M., & Seitz, F. (2021). The use of B-splines to represent the topography of river networks. *GEM: International Journal on Geomathematics*, *12*(1), 21. https://doi.org/10.1007/s13137-021-00188-w

Bosch, W., Dettmering, D., & Schwatke, C. (2014). Multi-mission cross-calibration of satellite altimeters: Constructing a long-term data record for global and regional sea level change studies. *Remote Sensing*, *6*(3), 2255–2281. https://doi.org/10.3390/rs6032255

Calmant, S., Crétaux, J. F., & Rémy, F. (2016). Principles of radar satellite altimetry for application on inland waters. *Microwave Remote Sensing of Land Surfaces: Techniques and Methods*, 175–218. https://doi.org/10.1016/B978-1-78548-159-8.50004-9

Calmant, S., & Seyler, F. (2006). Continental surface waters from satellite altimetry. *Comptes Rendus Geoscience*, *338*(14–15), 1113–1122. https://doi.org/10.1016/j.crte.2006.05.012

Carr, A. B., Trigg, M. A., Tshimanga, R. M., Borman, D. J., & Smith, M. W. (2019). Greater water surface variability revealed by new Congo River field data: Implications for satellite altimetry measurements of large rivers. *Geophysical Research Letters*, *46*(14), 8093–8101. https://doi.org/10.1029/2019GL083720

Cohen, S., Wan, T., Islam, M. T., & Syvitski, J. P. (2018). Global river slope: A new geospatial dataset and global-scale analysis. *Journal of Hydrology*, *563*(January), 1057–1067. https://doi.org/10.1016/j.jhydrol.2018.06.066

Cooley, S. W., Ryan, J. C., & Smith, L. C. (2021). Human alteration of global surface water storage variability. *Nature*, *591*(7848), 78–81. https://doi.org/10.1038/s41586-021-03262-3

Foerste, C., Bruinsma, S., Abrykosov, O., Lemoine, J.-M., Marty, J. C., Flechtner, F., et al. (2014). EIGEN-6C4 the latest combined global gravity field model including GOCE data up to degree and order 2190 of GFZ Potsdam and GRGS Toulouse. https://doi.org/10.5880/icgem.2015.1

Frappart, F., Calmant, S., Cauhopé, M., Seyler, F., & Cazenave, A. (2006). Preliminary results of ENVISAT RA-2-derived water levels validation over the Amazon basin. *Remote Sensing of Environment*, *100*(2), 252–264. https://doi.org/10.1016/j.rse.2005.10.027

Frasson, R. P. D. M., Pavelsky, T. M., Fonstad, M. A., Durand, M. T., Allen, G. H., Schumann, G., et al. (2019). Global relationships between river width, slope, catchment area, meander wavelength, sinuosity, and discharge. *Geophysical Research Letters*, *46*(6), 3252–3262. https://doi.org/10.1029/2019GL082027

Garambois, P. A., Calmant, S., Roux, H., Paris, A., Monnier, J., Finaud-Guyot, P., et al. (2017). Hydraulic visibility: Using satellite altimetry to parameterize a hydraulic model of an ungauged reach of a braided river. *Hydrological Processes*, *31*(4), 756–767. https://doi.org/10.1002/hyp.11033

Gleason, C. J., & Durand, M. T. (2020). Remote sensing of river discharge: A review and a framing for the discipline. *Remote Sensing*, *12*(7), 1–28. https://doi.org/10.3390/rs12071107

Gliński, J., Horabik, J., & Lipiec, J. (2011). Hydraulic gradient. In J. Gliński, J. Horabik, & J. Lipiec (Eds.), *Encyclopedia of agrophysics*. (p. 368). Springer. https://doi.org/10.1007/978-90-481-3585-1_680

Halicki, M., & Niedzielski, T. (2022). The accuracy of the Sentinel-3A altimetry over Polish rivers. *Journal of Hydrology*, *606*(April), 127355. https://doi.org/10.1016/j.jhydrol.2021.127355

Hannah, D. M., Demuth, S., van Lanen, H. A. J., Looser, U., Prudhomme, C., Rees, G., et al. (2011). Large-scale river flow archives: Importance, current status and future needs. *Hydrological Processes*, *25*(7), 1191–1200. https://doi.org/10.1002/hyp.7794

Herrmann, H., & Bucksch, H. (2014). Hydraulic gradient. In *Dictionary geotechnical engineering/wörterbuch geotechnik* (p. 697). Springer. https://doi.org/10.1007/978-3-642-41714-6_81759

Jasinski, M., Stoll, J., Hancock, D., Robbins, J., Nattala, J., Morison, J., et al. (2021a). *Algorithm theoretical basis document (ATBD) for inland water data products, ATL13, version 5, technical report* (Vol. 2). NASA Goddard Space Flight Center. https://doi.org/10.5067/RI5QTGTSVHRZ

Jasinski, M., Stoll, J., Hancock, D., Robbins, J., Nattala, J., Morison, J., et al. (2021b). ATLAS/ICESat-2 L3A inland water surface height, version 5 [Dataset]. Boulder, Colorado USA. https://doi.org/10.5067/ATLAS/ATL13.005

Jiang, L., Bandini, F., Smith, O., Jensen, I. K., & Bauer-Gottwein, P. (2020). The value of distributed high-resolution UAV-borne observations of water surface elevation for river management and hydrodynamic modeling. *Remote Sensing*, *12*(7), 1171. https://doi.org/10.3390/rs12071171

Julien, P. Y. (2018a). *River dynamics, chapter 11* (2nd ed.). Cambridge University Press. https://doi.org/10.1017/cbo9781139164016.009

Julien, P. Y. (2018b). Steady flow in rivers, chap. 5. In *River mechanics* (2nd ed.). Cambridge University Press. https://doi.org/10.1017/9781316107072.006

Kebede, M. G., Wang, L., Yang, K., Chen, D., Li, X., Zeng, T., & Hu, Z. (2020). Discharge estimates for ungauged rivers flowing over complex high-mountainous regions based solely on remote sensing-derived datasets. *Remote Sensing*, *12*(7), 1064. https://doi.org/10.3390/rs12071064

Langhorst, T., Pavelsky, T. M., Frasson, R. P. D. M., Wei, R., Domeneghetti, A., Altenau, E. H., et al. (2019). Anticipated improvements to river surface elevation profiles from the surface water and ocean topography mission. *Frontiers of Earth Science*, *7*(May), 1–13. https://doi.org/10.3389/feart.2019.00102

Lao, J., Wang, C., Nie, S., Xi, X., & Wang, J. (2022). Monitoring and analysis of water level changes in Mekong River from ICESat-2 spaceborne laser altimetry. *Water*, *14*(10), 1613. https://doi.org/10.3390/w14101613

LeFavour, G., & Alsdorf, D. (2005). Water slope and discharge in the Amazon River estimated using the shuttle radar topography mission digital elevation model. *Geophysical Research Letters*, *32*(17), 1491. https://doi.org/10.1029/2005GL023836

Mandlburger, G., Weiß, R., & Artz, T. (2020). Mapping of water surface levels and slopes with single photon LiDAR—A case study at the river Rhine. *The International Archives of the Photogrammetry, Remote Sensing and Spatial Information Sciences: ISPRS Archives*, *43*(B1), 57–64. https://doi.org/10.5194/isprs-archives-XLIII-B1-2020-57-2020

Manning, R. (1891). On the flow of water in open channels and pipes. *Transactions of the Institution of Civil Engineers of Ireland*, *20*, 161–207.

Markus, T., Neumann, T., Martino, A., Abdalati, W., Brunt, K., Csatho, B., et al. (2017). The Ice, Cloud, and Land Elevation Satellite-2 (ICESat-2): Science requirements, concept, and implementation. *Remote Sensing of Environment*, *190*, 260–273. https://doi.org/10.1016/j.rse.2016.12.029

Neumann, T. A., Martino, A. J., Markus, T., Bae, S., Bock, M. R., Brenner, A. C., et al. (2019). The Ice, Cloud, and Land Elevation Satellite-2 Mission: A global geolocated photon product derived from the advanced topographic laser altimeter system. *Remote Sensing of Environment*, *233*(September), 111325. https://doi.org/10.1016/j.rse.2019.111325

Niemeier, W. (2008). *Ausgleichungsrechnung: Statistische Auswertemethoden*. De Gruyter. https://doi.org/10.1515/9783110206784

O'Loughlin, F., Trigg, M. A., Schumann, G. J., & Bates, P. D. (2013). Hydraulic characterization of the middle reach of the Congo River. *Water Resources Research*, *49*(8), 5059–5070. https://doi.org/10.1002/wrcr.20398

Pitcher, L. H., Smith, L. C., Cooley, S. W., Zaino, A., Carlson, R., Pettit, J., et al. (2020). Advancing field-based GNSS surveying for validation of remotely sensed water surface elevation products. *Frontiers of Earth Science*, *8*(November), 1–20. https://doi.org/10.3389/feart.2020.00278

Rhoads, B. L. (2020). The vertical dimension of rivers: Longitudinal profiles, profile Adjustments, and step-pool morphology. In *River dynamics geomorphology to support management (chapter 13)*. Cambridge University Press. https://doi.org/10.4324/9781351218986-13

Ryan, J. C., Smith, L. C., Cooley, S. W., Pitcher, L. H., & Pavelsky, T. M. (2020). Global characterization of inland water reservoirs using ICESat-2 altimetry and climate reanalysis. *Geophysical Research Letters*, *47*(17), 1–10. https://doi.org/10.1029/2020GL088543

Sauer, V. B., & Turnipseed, D. P. (2010). Stage measurement at gaging stations. In *Techniques and methods (chapter 3-A7)*. U.S. Geological Survey. https://doi.org/10.3133/tm3A7

Scherer, D., Schwatke, C., Dettmering, D., & Seitz, F. (2020). Long-term discharge estimation for the lower Mississippi River using satellite altimetry and remote sensing images. *Remote Sensing*, *12*(17), 2693. https://doi.org/10.3390/rs12172693

Schumm, S. A. (2005). Valley morphology. In *River variability and complexity (chapter 12)*. Cambridge University Press. https://doi.org/10.1017/CBO9781139165440.015

Schwatke, C., Dettmering, D., Bosch, W., & Seitz, F. (2015). DAHITI—An innovative approach for estimating water level time series over inland waters using multi-mission satellite altimetry. *Hydrology and Earth System Sciences*, *19*(10), 4345–4364. https://doi.org/10.5194/hess-19-4345-2015

Sichangi, A. W., Wang, L., & Hu, Z. (2018). Estimation of river discharge solely from remote-sensing derived data: An initial study over the Yangtze river. *Remote Sensing*, *10*(9), 1385. https://doi.org/10.3390/rs10091385

Sichangi, A. W., Wang, L., Yang, K., Chen, D., Wang, Z., Li, X., et al. (2016). Estimating continental river basin discharges using multiple remote sensing data sets. *Remote Sensing of Environment*, *179*, 36–53. https://doi.org/10.1016/j.rse.2016.03.019

Sulistioadi, Y. B., Tseng, K. H., Shum, C. K., Hidayat, H., Sumaryono, M., Suhardiman, A., et al. (2015). Satellite radar altimetry for monitoring small rivers and lakes in Indonesia. *Hydrology and Earth System Sciences*, *19*(1), 341–359. https://doi.org/10.5194/hess-19-341-2015

Tapley, B. D., Ries, J. C., Davis, G. W., Eanes, R. J., Schutz, B. E., Shum, C. K., et al. (1994). Precision orbit determination for TOPEX/POSEIDON. *Journal of Geophysical Research*, *99*(C12), 24383. https://doi.org/10.1029/94JC01645

Tourian, M. J., Tarpanelli, A., Elmi, O., Qin, T., Brocca, L., Moramarco, T., & Sneeuw, N. (2016). Spatiotemporal densification of river water level time series by multimission satellite altimetry. *Water Resources Research*, *52*(2), 1140–1159. https://doi.org/10.1002/2015WR017654

Yamazaki, D., Ikeshima, D., Sosa, J., Bates, P. D., Allen, G. H., & Pavelsky, T. M. (2019). MERIT Hydro: A high-resolution global hydrography map based on latest topography dataset. *Water Resources Research*, *55*(6), 5053–5073. https://doi.org/10.1029/2019WR024873

Yamazaki, D., Ikeshima, D., Tawatari, R., Yamaguchi, T., O'Loughlin, F., Neal, J. C., et al. (2017). A high-accuracy map of global terrain elevations. *Geophysical Research Letters*, *44*(11), 5844–5853. https://doi.org/10.1002/2017GL072874

Zakharova, E., Nielsen, K., Kamenev, G., & Kouraev, A. (2020). River discharge estimation from radar altimetry: Assessment of satellite performance, river scales and methods. *Journal of Hydrology*, *583*(January), 124561. https://doi.org/10.1016/j.jhydrol.2020.124561